Ceramics International 50 (2024) 9682–9696

Contents lists available at ScienceDirect

Ceramics International

journal homepage: www.elsevier.com/locate/ceramint

Use of recycled carbon fibre as an additive in the manufacture of porous bricks more durable against salt crystallization

Laura Crespo-López [a,*], Chiara Coletti [b], Salvador Morales-Ruano [a,c], Giuseppe Cultrone [a]

[a] Department of Mineralogy and Petrology, Faculty of Sciences, University of Granada, Avda. Fuentenueva s/n, 18002, Granada, Spain
[b] Department of Geosciences, Università Degli Studi Di Padova, Via Giovanni Gradenigo, 6, 35131, Padova, Italy
[c] Andalusian Institute of Earth Sciences (IACT), University of Granada-CSIC, Avenida de las Palmeras, 4, 18100, Armilla, Granada, Spain

ARTICLE INFO

Handling Editor: Dr P. Vincenzini

Keywords:
Bricks
Carbon fibre
Recycling
Circular economy

ABSTRACT

Within the framework of the Sustainable Development Goals of the Agenda 2030, the circular economy is being promoted as a means of ensuring a sustainable use of resources and a reduction in the amount of waste produced. The aim is to reduce the demand for often scarce raw materials through the continuous reuse, recycling and regeneration of materials and products. This paper explores the use of carbon fibre from wind turbine blades as an additive in the production of new efficient bricks. Clay mixes with 0, 5 and 10 wt% additive were fired at three temperatures (800, 950 and 1100 °C) and the fired bricks were analysed from mineralogical and physical points of view to determine their suitability for use in the construction industry. The results show that carbon fibre improves the durability of the bricks, which became 16 % more porous as the firing temperature increased. However, the compressive strength of the bricks with 10 wt% carbon fibre was about 50 % lower than that of the control bricks made without additive. It is interesting to note that the distribution of the carbon fibres within the brick varies considerably and that they are shorter and wider in the core of the samples. These results could offer an alternative line for new product development in the brick industry. The bricks tested here are an example of a circular economy in which waste from one industrial process (wind turbine blades) is reused as an input in another (brick manufacture). The environmental benefits achieved are twofold: reduced demand for clay and recycling of decommissioned turbine blades, which are currently amassed in wind turbine graveyards.

1. Introduction

The circular economy is a sustainable economic model that aims to reduce resource consumption and waste generation by promoting the long-life usage, recycling and regeneration of materials [1,2]. By adopting circular practices, businesses and society can achieve long-term environmental and economic benefits, increasing resource efficiency and creating new employment opportunities in green industries [3,4]. Great efforts are currently being made to achieve sustainable development, inspired by the challenges outlined in the United Nations 2030 Agenda (Sustainable Development Goals- SDG) (UN General Assembly, [5]) in spite of these efforts, the Circularity Gap Report 2023 [6] reveals that the global economy is still only 7.2 % circular. It is therefore necessary for each economic sector to assess how circularity can best be achieved. Within the construction sector, one option that is currently being explored is the use of alternative and/or local raw materials in the manufacture of building materials. To this end, Gencel et al. [7,8], Er et al. [9], Crespo-López et al. [10], and Erdogmus et al. [11], have recently studied the use of inorganic residues such as industrial slags, water treatment slag, household glass and metallurgical wastes as additives in brick production. These additives modify certain physical properties of the fired bricks (above all, porosity, mechanical strength and durability). The aim of this paper is to support the brick industry in its search for suitable alternative raw materials that can be used in the manufacture of bricks, so reducing the amount of clay required. In this case, the study focuses on the carbon fibre waste from decommissioned wind turbine blades. In line with the SDG challenges (in particular SDG 12, "Responsible Consumption and Production" which has the most targets specifically addressing waste management), there are two main objectives, namely to reduce the demand and therefore the extraction of natural resources and to reuse and recycle as raw materials the waste produced by other anthropogenic activities. Successful application of alternative raw materials of this kind would also have socioeconomic benefits in terms of cost savings.

* Corresponding author.
E-mail address: lcrespo@ugr.es (L. Crespo-López).

https://doi.org/10.1016/j.ceramint.2023.12.287
Received 25 September 2023; Received in revised form 12 December 2023; Accepted 21 December 2023
Available online 26 December 2023

Wind is a competitive, clean energy source and its industry is booming. If the wind targets set out in REPowerEU (2022) [12], the EU's energy security strategy, are successfully met, a massive 65 billion cubic meters of gas could be saved. Apart from reducing greenhouse gas emissions (GHG), this would also make Europe self-sufficient in terms of energy production and less reliant on imported fossil fuels. Wind is an increasingly stable form of power supply. New onshore wind farms now operate at capacity factors of 30–45 %, and new offshore wind farms at 50 % [13,14]. Wind power does not emit any CO_2, SO_x, NO_x, or metal particles [15]. It emits ~95 % less CO_2 than gas-based electricity production and ~98 % less CO_2 than coal-based production [16] and consumes very little water. Wind meets 15 % of electricity demand in the EU as a whole and much more in certain countries: Denmark 44 %; Ireland 31 %; Portugal 26 %; Spain 24 %, and Germany 23 % [17–19]. The International Energy Agency (IEA [20]) expects wind to be the first source of power in Europe by 2027. The standard lifetime of a wind farm is around 20–25 years. When wind turbines reach the end of their life, project developers must take them down and restore the site to its pre-existing condition. According to WindEurope 2021 [21], the European Wind Energy Association (EWEA, 2013) [22] and Recycling International [23], around 14,000 blades may have to be dismantled across the continent in the next five years, which would create between 40,000 and 60,000 tonnes of waste.

Wind-turbine blades are typically composed of several materials, including glass fibre, carbon fibre, carbon/glass (hybrid) fibre, reinforced polymer composites and foam. The exact combination of materials used in wind turbine blades may vary depending on the manufacturer and the wind turbine model [24]. Carbon fibre is the typical material used in the blades on the larger, higher-capacity turbines [25]. It is known for its high strength, stiffness and durability, making it an ideal material to support the load and stress experienced by blades during operation [26]. Another benefit is that it is lighter than other materials, so ensuring that the blades are lighter and more energy-efficient [27,28]. The use of carbon fibre also allows longer blades to be made, which increases the amount of energy that can be produced with each turn of the turbine [29]. Although carbon fibre is expensive, its use as the raw material in wind turbine blades can lead to increased efficiency and durability of the turbines, so reducing long-term maintenance and operating costs [30]. The wind industry has committed to recycling or recovering 100 % of decommissioned wind turbines by 2025 and work is currently underway to boost recycling through different technologies, e.g. mechanical recycling, which involves shredding materials so that they can be reused for example as filler material in building materials or plastics; thermal recycling, which entails incinerating the blades to break down the composites, producing energy in the process; or chemical recycling, which uses solvents and thermal processes to separate the resins from the fibres so that both materials can be reused [24,26,31]. In this regard, the construction industry can play an important role in the recycling of these blades, by promoting the production of new materials. Yazdanbakhsh et al. [32] investigated the addition of 5–10 % volume of slender elements from wind turbine blades (known as "needles") to a concrete mix. Results revealed no negative effects on the steadiness or workability of the new concrete or on its tensile, compressive and flexural strength.

This paper aims to offer the wind industry a new perspective on blade waste recycling by using this residue as an additive in the production of bricks. It could also provide an opportunity for the brick industry to test the feasibility of using carbon fibres in the manufacture of what could potentially be high-performance materials. Carbon fibre is very light, so transport costs would be lower than with traditional bricks, and its use in the brick production process would provide direct benefits for the environment by reducing the depletion of clayey soils, which are non-renewable natural resources [33,34].

This paper breaks new ground in the brick industry sector, because although there have been studies that investigated the addition of carbon fibre to concrete for the construction of structural elements such as beams and columns [35–37], no specific research has been conducted on the reuse of carbon fibre from wind turbine blades in brick manufacture. With this in mind, the aim of this research is to produce a new type of brick which i) is environmentally friendly, ii) uses fewer raw materials, iii) contributes to the elimination of waste and iv) meets the relevant standards in terms of its physical-mechanical properties for use in the construction industry.

2. Materials and method

2.1. Geological context and supply of raw materials

Bricks were made by mixing clayey materials from Viznar and Guadix (Granada, Spain). In geological terms, Viznar is part of the Granada basin, while Guadix belongs to the Guadix basin. Both basins are part of the central area of the Betic Cordillera. The clayey material from Guadix was deposited in the Middle-Late Pleistocene during the last stages of basin infilling, while the clay from Viznar was deposited during the late Turolian in a lacustrine environment with alluvial sediments (conglomerates and sands), deltaic sediments, small calcarenitic platforms and other minor materials from Sierra Nevada and Sierra Arana [38].

This work was carried out in partnership with the company Tesela, Materiales, Innovación y Patrimonio S.L. (Granada, Spain), who supplied carbon fibre powder (CF) from the blades of decommissioned wind turbines from wind-farms in Spain, and with the brick manufacturer Cerámica Castillo Siles (Granada, Spain), who supplied the clayey materials.

2.2. Traditional brick production

In this study, the bricks were made using a mixture of clayey materials from Viznar and Guadix in proportions of 3/5 and 2/5 by weight, respectively. These proportions were chosen on the recommendation of the brick manufacturer who supplied the raw materials, because in his experience they produced the most workable mix and the best-quality end products. Fig. S1 shows the different steps in the brickmaking process. Several kilograms of the two clayey materials from Viznar and Guadix were removed from piles of clay in the brick factory using a shovel. All coarse rock fragments and plant roots were discarded. Once in the laboratory, the clayey materials were sieved and fragments of over 1.5 mm in size were removed. The two types of clay were then mixed together in the proportions mentioned above. With a view to using as much residue as possible without affecting the workability of the clay mixture, and as there was no previous bibliography to follow, it was decided to use 5 and 10 wt% of carbon fibre powder (CF). With higher amounts of carbon fibre, the clayey mass became less workable. The addition of carbon fibre means that less clay is required to produce the bricks (Table S1). The maximum amount of added CF was set at 10 wt%, given that as CF is a very lightweight material in relation to its volume, the addition of over 10 wt% CF could have prevented the residue from mixing properly with the clayey materials. The clay and CF mixtures were then mixed with water and moulded in moistened wooden moulds of 15 × 20 × 4 cm (Fig.S1 A and S1B). Table S1 shows the proportions of clayey material, carbon fibre powder (by weight percentage, wt.%) and water used in each mix design. A control group (CF0) of bricks with no added carbon fibre powder was also prepared.

Moulds were removed after 1 h and the clayey pastes were cut into ~4 cm edge cubes using a stretched cotton thread and left to dry (Fig. S1C). Once the samples had dried, they were fired in a Herotec CR-35 electric oven at 800, 950 and 1100 °C (Fig. S1C). These three temperatures were selected on the following basis. The intermediate temperature (950 °C) was chosen because it is one of the most commonly used in the brick industry (the brick manufacturer who provided the raw materials fires his bricks at this temperature). The other two were chosen to enable the analysis of the mineralogical, textural, physical and

durability changes in the bricks with and without added CF over a range of 300 °C. Table S2 offers a summary of the samples analysed in this paper. The temperature inside the oven was initially kept constant for 1 h at 100 °C to eliminate any residual moisture in the samples. Then, the temperature was increased at a rate of 2 °C/min (heating). Once the desired temperature had been reached, the oven was kept at a constant temperature for 3 h (soaking). Finally, it was turned off and the samples were left to cool slowly (cooling). They were not removed from the oven until the next day. After removal from the oven, the bricks were immersed in water for about 1 h to prevent possible "lime blowing" due to the presence of lime grains [39].

2.3. Analytical techniques

2.3.1. Chemistry, mineralogy and texture of the raw materials and fired bricks

The granulometry of the raw material and of the CF was determined using a Galai CIS-1 laser gauge that uses laser diffraction to measure the range of the particles after 10 s sonication in water over a 0.02–1500 μm range. The thermal decomposition of the clayey material up to 950 °C was carried out using a METTLER-TOLEDO TGA/DSC1 thermogravimetric analyser coupled with differential scanning calorimetry (TG-DSC). About 20 mg of sample was deposited on an Al crucible and analysed in a flowing air atmosphere (50 ml/min) at a heating rate of 20 °C/min. The components of the carbon fibre in the IR spectrum were identified using a Fourier transform infrared spectroscopy with an attenuated total reflectance sample holder (ATR-FTIR), in a frequency range of 4000-400 cm^{-1} and with a step size of 0.50 cm^{-1}. X-ray fluorescence (XRF) was used to determine the major elements in the clayey material and in the CF with a PANalytical Zetium compact spectrometer with an Rh anode and a 4 kV X-ray generator. 5 g per sample were milled to powder in an agate mortar and then analysed. The Loss On Ignition (LOI) was determined by burning the samples at 1000 °C for 1 h. The mineralogical composition of the raw material and the fired bricks was determined by powder X-ray diffraction (PXRD) using a PANalytical X'Pert PRO diffractometer. The working conditions were as follows: CuKα radiation, 45 kV voltage, 40 mA current, 3–70° 2θ exploration range, 0.1 2θ s^{-1} goniometer speed. Mineral phase identification was first performed using the PANalytical X'pert Highscore Plus 3.0 software, matching the experimental diffraction peaks with those from the Joint Committee for Powder Diffraction Standards (JCPDS) PDF-2 database. Quantitative estimations were also performed by adding 10 wt% internal standard α-Al_2O_3 to the powder samples and detecting the peaks using open-source Profex-BGMN software, which has dedicated fitting functions [40–43] for Rietveld refinements [44]. The goodness-of-fit of the refinements (GoF) were between 1.68 and 1.87.

The petrographic features of the fired bricks were observed by means of polarized optical microscopy (POM). Observations under plane- and cross-polarized light were carried out on polished thin sections using a Carl Zeiss Jenapol-U microscope equipped with a Nikon D7000 digital camera. Detailed observations of the morphology of the carbon fibres and of the texture, pore morphology and degree of vitrification of the fired bricks were made using a high-resolution field emission scanning electron microscope (FESEM) Carl Zeiss SMT (AURIGA series) coupled with energy dispersive X-ray analysis (EDS). The carbon fibres and brick fragments were carbon-coated prior to their observation under FESEM.

2.3.2. The pore system of the bricks

The pore system of the fired bricks was investigated using hydric and porosimetric tests (Table S3). To this end, free (Ab, at atmospheric pressure [45]) and forced (Af, under vacuum) water absorption and drying tests (Di, [46]) were carried out (according to the relevant standards, see Table S3). These tests enabled us to determine the degree of pore interconnectivity (Ax), the capillary rise (C) [47], the saturation coefficient (S) [48], the apparent (ρ_a) and real (ρ_r) densities and the open porosity (Po) (Equations 1-9, Table S3) [49,50]. Hydric tests were performed under controlled thermo-hygrometric conditions (20 °C and 60 % RH) using deionized water. Three samples per brick (~4 cm edge cube) group were analysed.

The pore system of the bricks within a range of 0.002–200 μm was analysed by mercury intrusion porosimetry (MIP) using a Micromeritics Autopore V 9600 porosimeter with a mercury-brick contact angle of 130°. Open porosity (Po_{MIP}) (Equations 6, Table S3) [49,50] and specific surface area (SSA) were calculated.

2.3.3. Durability of the bricks

Fifteen salt crystallization cycles were performed to assess a theoretical degradation that could affect the lifetime of the bricks according to the UNE-EN 12370 standard [51]. This test reproduces the decay that the bricks may undergo due to the dissolution and recrystallization of soluble salts within their porous systems. Three samples per brick type were used for this test.

2.3.4. Mechanical behaviour (Cs)

In the analysis of compressive strength (Cs), three samples measuring 1.5 × 1.5 × 6 cm were tested for each brick type (Equation 10, Table S3) [52]. The compressive strength of these samples was measured using a Controls Uniframe T1192 electromechanical universal tester, equipped with 100 kN and 25 kN load cells and a loading rate 0.6 of mm/min. This device was specially designed for measuring the compressive strength of small bricks.

2.3.5. The compactness of the bricks

The ultrasound propagation velocity of compressional (V_p) and shear (V_s) waves was measured with a Panametrics HV Pulser/Receiver 5058 PR coupled with a Tektronix TDS 3012B oscilloscope. It was measured in accordance with the ASTM D2845 [53] (Equations 11, Table S3) standard for dry test samples using transducers of 1 MHz. These data were used to obtain information on the compactness of the bricks. A viscoelastic gel was applied to ensure good coupling between the transducers and the brick samples. V_p and V_s were measured in the three perpendicular directions on cubic samples. Once the ultrasound velocities had been determined, total anisotropy (ΔM), the Poisson coefficient (ν) [54,55], and the Young (E) [54,55], Shear (G) [56] and Bulk (K) [54] moduli were calculated (Equations 12–15, Table S3).

The Leeb Hardness (LH) tester PCE-2500 N was used to measure the surface hardness of the bricks using a rebound hammer. Ten linear measurements were made from one edge of each brick to the opposite side passing through the centre. The harder the surface of the material, the higher the rebound velocity [57].

2.3.6. Colour

Colour measurements were performed to quantify the lightness (L*) and chromatic coordinates (a* and b*) of the fired bricks [58]. A Konica Minolta CM-700d spectrophotometer was used. Illuminant D65, 10° observer angle and 8 mm measurement area were used. Nine measurements per sample were performed. The total colour variation (ΔE) between the control bricks and those with added CF was calculated (Equation 16, Table S3).

3. Results and discussion

3.1. Grain size distribution, thermogravimetry and chemistry of the clayey material and CF

The granulometric analysis shows that the clayey material has a unimodal particle size distribution with a maximum peak at 23.2 μm (Fig. 1A). As expected, the carbon fibre (CF) curve has a shorter size distribution compared to the clayey material. This curve is bimodal, although there is a dominant maximum peak at 14.1 μm and a smaller one at 102.5 μm. Thermal analysis of the clayey material (Fig. 1B) shows a weight loss of 5 % at 86 °C due to the loss of hygroscopic water [59]. At

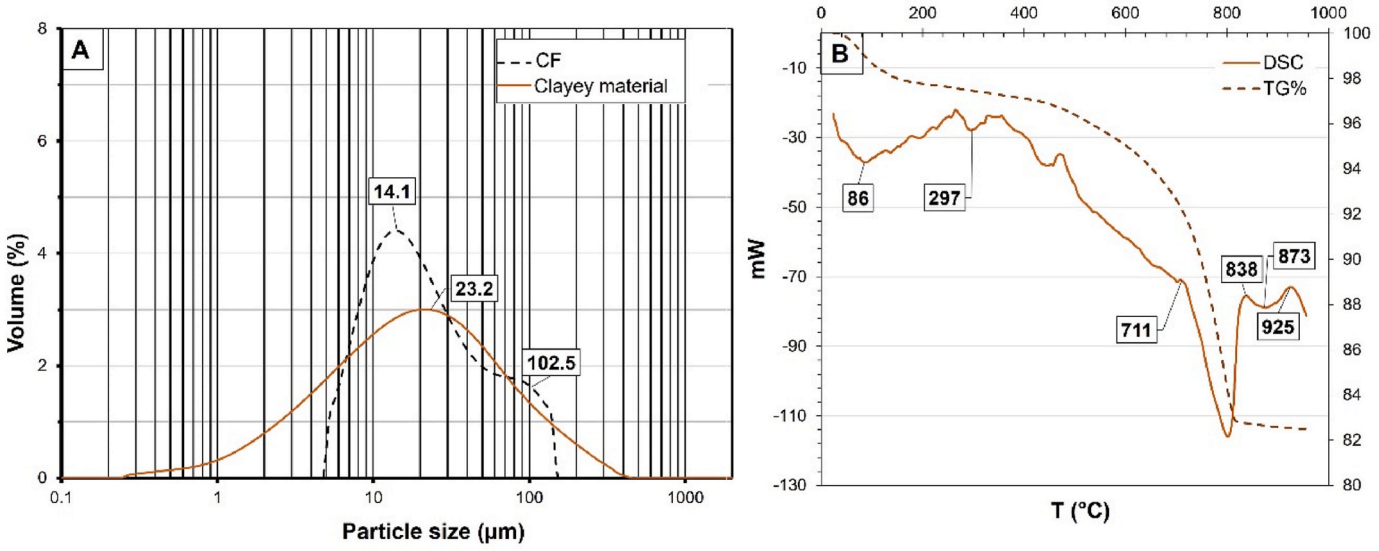

Fig. 1. Grain size distribution of the raw materials (clayey material and carbon fibre, CF) (A) and TG-DSC analysis of the clayey material (B). A) Particle size (in µm) vs. volume (in %). B) Temperature (in °C) vs. weight loss (right ordinate, in %) and differential scanning calorimetry (left ordinate, in mW).

297 °C there is an inflection in the curve corresponding to the combustion of organic matter [60,61]. At ~500 °C, a gradual dehydroxylation of the phyllosilicates begins to occur, which continues up to 711 °C [62,63]. Between 711 °C and 800 °C, the main weight loss of around 13 % occurs. This is linked to the decomposition of carbonates and the release of CO_2 [62,64,65]. The clayey material starts losing weight again at ~840 °C, probably due to further dehydroxylation of the phyllosilicates [66–68]. Finally, an exothermic peak is observed at 925 °C due to the formation of new crystalline phases, which will later be identified using PXRD analysis.

The IR spectrum obtained from the carbon fibre was compared with other spectra reported in the literature. Table 1 shows a summary of the bands identified, their attribution and references. The IR spectrum revealed that at some earlier stage the carbon fibre had been carbonised at a temperature of approximately 850 °C [69–71], probably in order to make the blades stronger and more durable. Fig. 2 illustrates the infrared spectra of the carbon fibres, where the larger and thinner bands in the range 1300–1800 cm^{-1} show a chaotic trend due to the presence of several compounds together with the carbon fibre. A peak at 1730 cm^{-1} was evidence of the ester (arachidyl dodecanoate) functional group [72]. Ketone and carboxylic acid C═O peaks were centred at 1705 cm^{-1} [73]. The peak of benzoic acid was present at a lower wavenumber, 1640 cm^{-1}, probably because of the aromaticity of the compound [74]. This peak is quite high due to the carbonisation detected in the sample.

Table 1
FTIR bands identified for CF, their attribution and references.

Bands identified (cm^{-1})	Attribution	References
450–600	free water	[76]
965	ammonia	[77]
1250–2000	free water	[76]
1300	sulphur dioxide	[76]
1510	phenol	[78]
1713	ε- caprolactam	[79]
1730	ester	[72]
1705	ketone and carboxylic acid	[73]
1640	benzoic acid	[74]
2000–2100	carbon monoxide	[80]
2100–2051	carbonyl sulphide	[77]
2298	carbon dioxide	[80]
2389–2667	monomer	[51]
3500–4000	free water	[76]
3570–3750	carbon dioxide	[80]

Peaks at 2389 and 2667 cm^{-1} are related to C–H stretching of the monomer units [75].

Other compounds detected in the FC sample were: free water (H_2O: 450–600 cm^{-1}; 1250–2000 cm^{-1}; 3500–4000 cm^{-1}) [76], carbon dioxide (CO_2: 3570–3750 cm^{-1}; 2298 cm^{-1}; 631–779 cm^{-1}), carbon monoxide (CO: 2000–2100 cm^{-1}) [80], carbonyl sulphide (COS: double peaks at 2100 and 2051 cm^{-1}), ammonia (NH_3: 965 cm^{-1}) [77] and sulphur dioxide (SO_2: 1300 cm^{-1}) [76]. The degradation of thermoplastic products (mainly the peak of ε-caprolactam [79] at 1713 cm^{-1}) and the release of phenol at 1510 cm^{-1} [78] were also observed. In relation to these compounds detected by FTIR, Cusidó et al. [80] and Cremades et al. [78] studied the hazardousness of the gases emitted during the firing of ceramics made with additives, recommending the use of technologies that minimize the emission of pollutants that are dangerous for human health. In this case, the addition of 5–10 wt% carbon fibre would increase CO_2 emissions during the firing process, as explained below.

Table 2 shows the chemistry of the clayey material and the carbon fibre (CF). The raw material is rich in SiO_2 and has a high Al_2O_3 content. The presence of CaO (9.23 %) and MgO (2.82 %) is a sign of its carbonate content. The carbon fibre is composed almost exclusively of carbon, which is consumed during calcination of the sample, so explaining the very high loss on ignition (LOI) of over 99 %. The calcination of carbon fibres results in the emission of CO_2 into the atmosphere, an issue that must be taken into account if this residue is to be used in the brick industry, as these factories are subject to carbon tax and CO_2 emission restrictions. Furthermore, the resin residues associated with the fibres will increase the total organic carbon in the flue gas [80]. However, the use of carbon fibres as an additive in brick production is more environmentally friendly in terms of air pollution than other possible methods for dealing with decommissioned turbine blades such us incineration, pyrolysis, or chemical recycling [81–83]. Cameán 2011 [84] and Rodríguez Vazquez [85] have shown that if metals such as Fe, Ti and Al are present, even in small amounts, in the clayey material, they can promote the graphitization of carbon fibres during the firing process.

3.2. Mineralogy of the clayey material and fired bricks

Rietveld refinement of PXRD analysis reveals that the clay mixture is rich in quartz (41 wt%) (Table 2), which confirms the high SiO_2 content detected by XRF (see Table 3). Other phases detected include carbonates

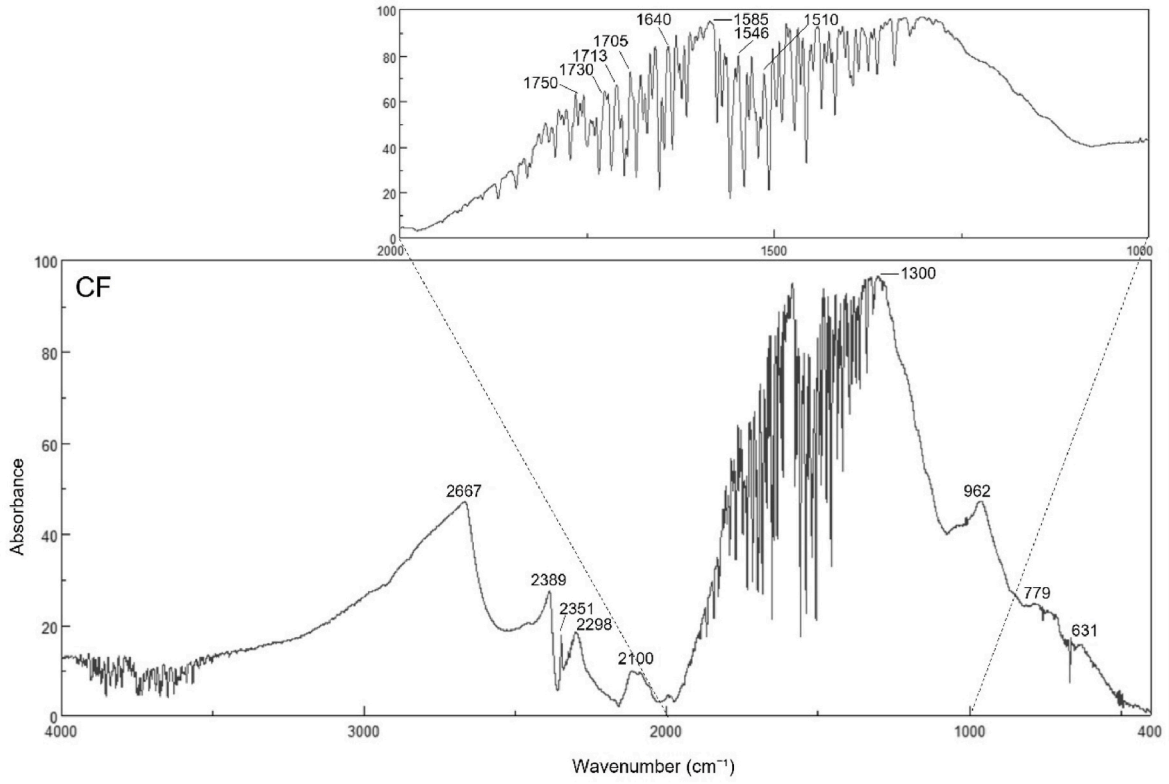

Fig. 2. Infrared spectrum of the carbon fibre used in this study. The range of the spectrum from 2000 to 1000 cm^{-1} has been marked to highlight the presence of other components in the carbon fibre sample.

Table 2
Chemical analysis of mayor oxides (in wt.%) in the raw material and CF.

	SiO_2	Al_2O_3	Fe_2O_3	MnO	MgO	CaO	Na_2O	K_2O	TiO_2	P_2O_5	LOI
Clayey material	48.78	15.97	5.69	0.07	2.80	9.43	1.27	2.70	0.83	0.16	12.40
CF	0.47	0.08	0.03	–	0.02	0.32	0.02	0.03	–	0.03	99.13

Table 3
Mineralogical characterization by PXRD of the clayey material and the fired bricks with or without added CF. Data is provided in weight %. Abbreviations of minerals according to Warr 2020 [89]: Sme: smectite; Ilt: illite; Pg: paragonite; Kln: kaolinite; Chl: chlorite; Mc: microcline; Qz: quartz; Cal: calcite; Dol: dolomite; Hem: hematite; Or: orthoclase; Sa: sanidine; Gh: gehlenite; An: anorthite; Mul: mullite; Wo: wollastonite; Di: diopside; Amph: amorphous phase.

	Sme	Ilt	Pg	Kln	Chl	Mc	Qz	Cal	Dol	Hem	Or	Sa	Gh	An	Mull	Wo	Di	Amph	ERROR
Clay mat.	3	12	2	2	1	8	41	6	5	5	–	–	–	–	–	–	–	13	±5
CF0/800	–	19	–	–	–	–	40	4	–	4	4	–	–	–	–	–	–	30	±2
CF5/800	–	18	–	–	–	–	39	4	–	2	2	–	–	–	–	–	–	35	±3
CF10/800	–	16	–	–	–	–	32	5	–	1	3	–	–	–	–	–	–	42	±4
CF0/950		16	–	–	–	–	31	–	–	5	–	1	7	12	–	–	–	30	±2
CF5/950	–	10	–	–	–	–	32	–	–	2	–	2	3	14	–	–	–	37	±2
CF10/950	–	14	–	–	–	–	20	–	–	1	–	1	7	11	–	–	–	47	±3
CF0/1100	–	–	–	–	–	–	26	–	–	5	–	2	4	19	3	2	9	33	±1
CF5/1100	–	–	–	–	–	–	23	–	–	1	–	2	2	22	3	2	10	41	±2
CF10/1100	–	–	–	–	–	–	24	–	–	0	–	3	2	22	4	3	12	48	±3

(calcite and dolomite, 11 wt%), K-feldspar (microcline 8 wt%), hematite (5 wt%) and phyllosilicates (smectite, illite, paragonite, kaolinite and chlorite, 21 wt%). The CaO and MgO content analysed by XRF (12 %, Table 2) is in accordance with the carbonate content determined by PXRD. Paragonite is a common phyllosilicate in the inner areas of the Betic Cordillera and is found in the raw material from Guadix [86,87]. For its part, the clay from Viznar is rich in carbonates from the different geological formations in the Granada Depression [88]. The amorphous phase content in the clay mixture is 13 wt%.

Table 3 shows the changes in the mineralogy of the bricks after firing. These changes are more obvious at 1100 °C with the crystallization of high-temperature silicates, the increase in background noise due to the vitrification of the samples [67] and more extensive development of a graphite-type crystalline structure in the samples with added CF. The amorphous phase content (in wt.%) increases in line with the firing temperature and with the percentage of CF, reaching its highest value in the samples fired at 1100 °C and with 10 wt% CF. At the three firing temperatures studied (800, 950 and 1100 °C), quartz is the most abundant phase (ranging from 41 to 20 wt%), while hematite and feldspars *s.l.* are detected in all the samples. At 800 °C, all the

phyllosilicates have disappeared with the exception of a dehydroxylated illite. The fired bricks have a higher illite content than the raw unfired bricks. This seems to be due to an overestimation of this phase due to the decomposition of the other phyllosilicates and their absence in the phase count (they accounted for 8 %, Table 3). Illite can still be detected at 950 °C, although the reflection (001) at 10 Å is lower than that observed in the clay mixture, suggesting a lower concentration of this phase. Dehydroxylation can influence the properties of the surrounding material, such as the strength and porosity of the fired brick [90]. Calcite is detected in very small amounts at 800 °C (~4 wt%) and disappears at higher temperatures, while dolomite has already disappeared at 800 °C (Table 2). Microcline detected in the clayey material converted into its polymorphs, i.e. orthoclase at 800 °C and sanidine at 950 °C and 1100 °C [91]. The hematite concentration decreases with increasing firing temperature in the samples made with added CF, reaching values of <1 wt% in CF10/1100 as compared to 5 wt% in CF0/1100 (Table 2). The decomposition of carbonates and their reactions with quartz and other silicates leads to the appearance of new Ca- (and Mg-) silicates such as gehlenite at 950 °C and wollastonite, anorthite and diopside at 1100 °C. Another new phase, mullite, is identified at 1100 °C. The appearance of these phases is manifested in the exothermic peak observed in TG-DSC analysis at 925 °C (Fig. 1B).

3.3. Texture and microtexture of the fired bricks

The observations under MOP of the bricks made with and without carbon fibre revealed the presence of fragments of mica-schists, gneiss and quartz grains with undulose extinction with a maximum length of about 1 mm. At 800 °C these fragments are homogeneously distributed in an orange matrix (Fig. 3A) forming the temper of the bricks. With the addition of carbon fibre, the matrix becomes browner in colour and disoriented carbon fibres are observed as part of the matrix (Fig. 3B and C). These fibres probably encourage the development of a reducing environment in the oven and the formation of “black core”. At 800 °C, other minerals can also be observed. The carbonate grains are partially decomposed and have lost their typical high interference colour (Fig. 3B). Phyllosilicates appear unaltered and often have a preferential orientation due to the pressure exerted during kneading. Pores are mainly elongated and follow the same orientation as planar minerals. At 950 °C, the matrix is slightly darker (Fig. 3D) due to the gradual vitrification and even more so in the samples with added CF (Fig. 3E and F). The phyllosilicates become less birefringent, and carbonates are totally decomposed. In the bricks with carbon fibre (Fig. 3E and F), it seems that the fibres start to form clumps and orient themselves slightly. Many of the fibres were severely affected, and some even disappeared, leaving imprints in their place. At 1100 °C, due to the high firing temperature, the pores become ellipsoidal-to-rounded and the matrix becomes dark (Fig. 3G, H and I). This change is more noticeable in the samples made

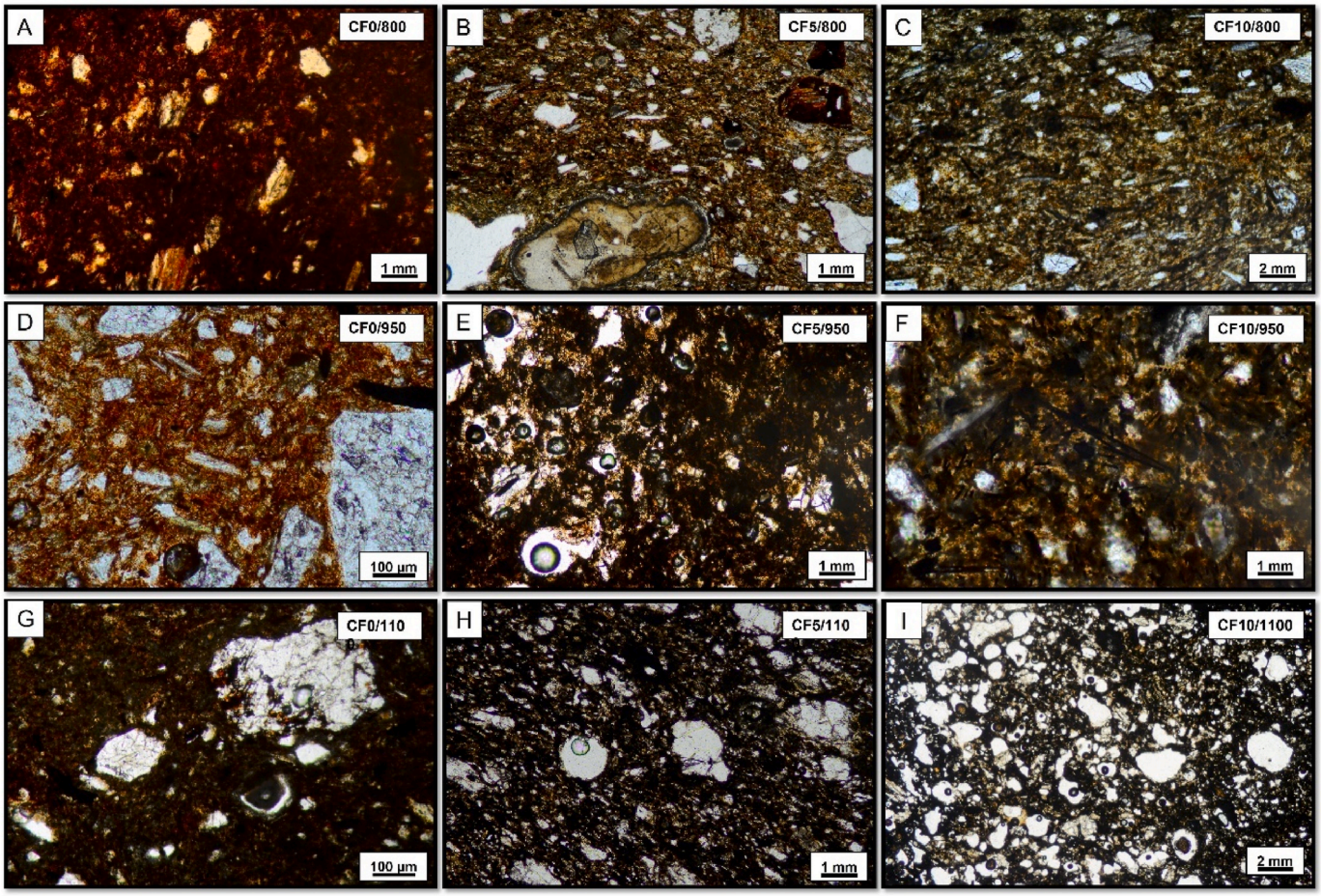

Fig. 3. Optical microscopy images of bricks with or without added carbon fibres fired at 800, 950 and 1100 °C, as observed in plane-polarized light. A) orange matrix of sample FC0/800; B) and C) brown matrix of the samples fired at 800 °C with added CF (CF5/800 and CF10/800, respectively). D) phyllosilicate grains with a preferential orientation in the FC0/950 sample; E) and F) the matrix is slightly darker due to the gradual vitrification and the presence of imprints of CF; G) dark matrix in the CF0/1100 sample; H) and I) rounded pores in the samples fired at 1100 °C with added CF (CF5/1100 and CF10/1100). (For interpretation of the references to colour in this figure legend, the reader is referred to the Web version of this article.)

with CF. This is probably because of the combustion of fibres (remember the high LOI of CF weighed at 1000 °C in Table 1), which brings more heat into the matrix. In these samples, the development of sandwiched structures, i.e. black cores, is more evident. The phyllosilicates have lost their birefringence and have a whitish interference colour. According to Pask & Tomsia [92] and Rodríguez Navarro et al. [93], the kaolinite and illite have probably been replaced by mullite, as also suggested by the PXRD results (Table 3).

Fig. 4 offers a schematic image of the distribution and orientation of the imprints of the carbon fibres and pores in the matrix of sample CF10/1100. Three concentric areas (A, B and C) can be distinguished. In the outer area of the sample (A zone), which has a more orangey colour, a small amount of randomly arranged imprints can be observed under the microscope, together with small, rounded pores. In the middle area (B zone), the imprints are shorter and thicker than those observed in the outer area and tend to orient themselves. In the core of the sample (C zone), the imprints remain thick but increase in length forming oriented aggregates in bundles. The additional heat provided by the combustion of the fibres is probably responsible for these textural changes. According to Cameán [85], it is possible that carbon fibres are oriented by the pressure applied during the preparation of handmade bricks prior to firing, an effect that becomes more intense as more carbon fibres are added.

The FESEM observations were made on detached particles of carbon fibre before it was kneaded with the clayey material (Fig. 5) and on fragments of the bricks made with 0 wt% and 10 wt% CF fired at 800 °C (Fig. 6). The aim was to highlight the textural differences in the brick matrix caused by the addition of the highest amount of CF. Although this question was not analysed in our study, previous researchers argued that the microstructural changes resulting from the addition of CF could have improved the thermal properties of bricks, and in particular their thermal conductivity [94]. Fig. 6 shows a general view of the carbon fibres used to make the bricks. As expected, this waste is not only composed of elongated fibres but also contains rough and irregular aggregates (Fig. 5A–C). EDS analysis confirms the presence of C and O in the carbon fibres. These aggregates probably come from the reinforcing foam used in the construction of the blades [95–97]. They are very sensitive to increases in temperature, forming pores in the fired bricks. The carbon fibres range in length from 5 to 90 μm and have a diameter of around 6–9 μm. The surface of the fibres appears striated (Fig. 5D).

The addition of carbon fibres to the clayey mix results in a partial change in the texture of the fired bricks and the matrix becomes quite heterogeneous (Fig. 6A, CF0/800 and Fig. 6C, CF10/800). In both groups of bricks (CF0 and CF10), the phyllosilicate grains maintain their lamellar habit, although the lamellae tend to separate along their basal plane due to dehydroxylation (Fig. 6B) [98]. Carbonate grains are

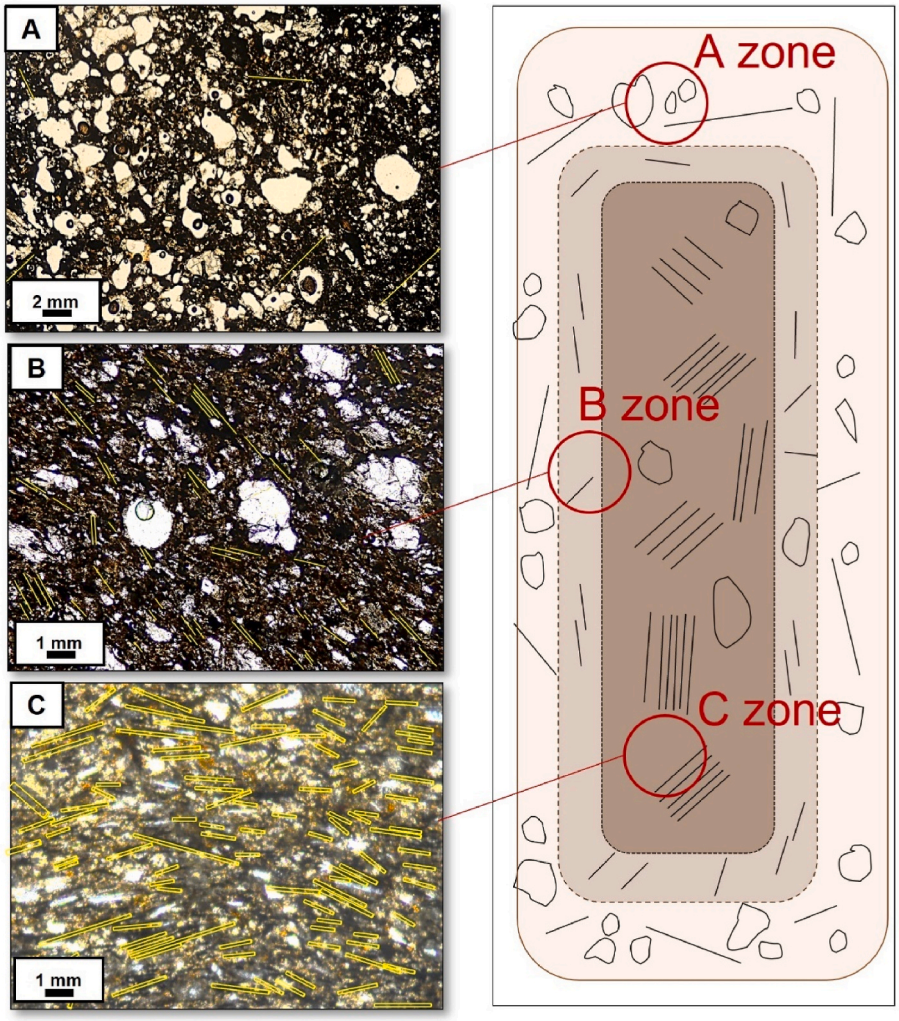

Fig. 4. Left – Optical microscopy images in plane-polarized light. The fibres and their imprints are highlighted in yellow. Right – schematic view of a thin section of the CF10/1100 brick. Moving inwards from the outside to the core of the brick, three quite distinct zones can be observed: Zone A, the outermost zone, corresponds to MOP image A, zone B to image B and zone C, the innermost area, to image C. (For interpretation of the references to colour in this figure legend, the reader is referred to the Web version of this article.)

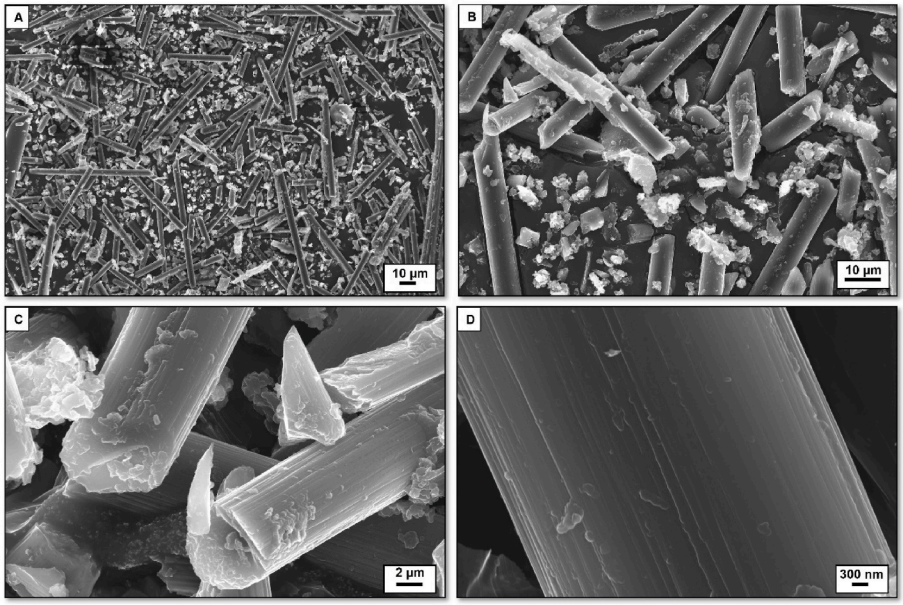

Fig. 5. FESEM secondary electron images of carbon fibres added to the clayey material to make the bricks. A) General view of carbon fibres and other particulate matter from wind turbines; B) unidentified aggregates with irregular morphology together with fibres; C) detailed image of the cylindrical morphology of the carbon fibres; D) detail of the surface morphology of a carbon fibre highlighting the presence of striae on the surface.

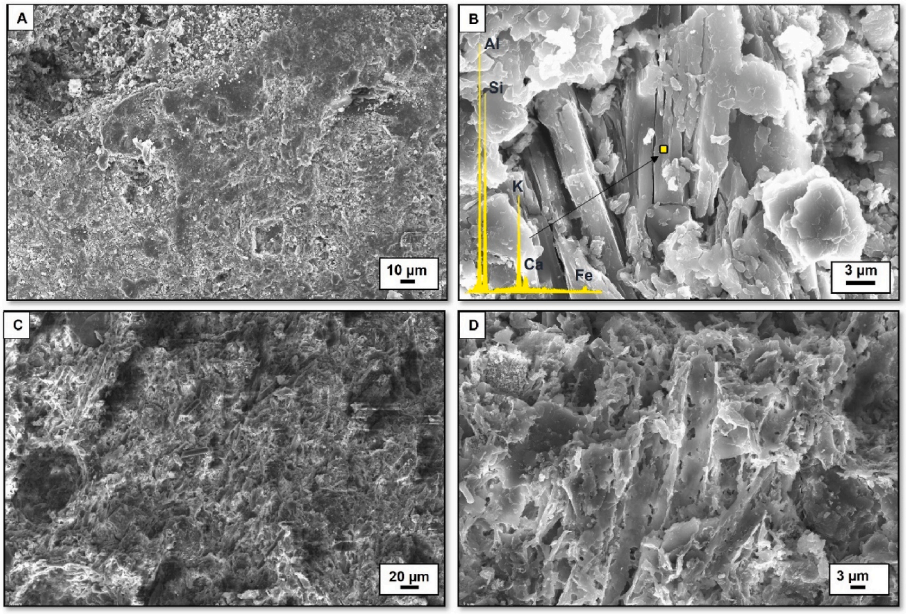

Fig. 6. FESEM secondary electron images.: A) General view of the texture and porosity of the sample CF0/800; B) dehydroxylation of a phyllosilicate grain along (001) planes in CF0/800 (the EDS of the phyllosilicate can be seen in the inset); C) general view of the texture and porosity of the sample CF10/800; D) imprints left by carbon fibres in sample CF10/800.

partially decomposed, confirming MOP observation and PXRD data. The carbon fibres in the fired bricks, when visible, show a change in their morphology compared to the unfired fibres (Fig. 6D), as a result of firing. The striae observed on the unfired fibres (Fig. 5D) have disappeared or thinned out. It is also possible to corroborate the changes in the size of the fibres noted during MOP observations. At 800 °C they have already started to thicken and shorten and by 1100 °C they are completely calcined. At 800 °C some fibres have disappeared due to combustion, leaving imprints in the matrix of the brick (Fig. 6D), as already observed under POM. At the same time, greater porosity and irregular-shaped pores can be distinguished in the bricks made with CF. This may be linked to the burning of carbon fibres and reinforcing foam observed under FESEM (Fig. 5B).

The orientation of the CF occurs because they are oxygen-rich organic compounds that develop a structure with aliphatic crosslinks that provide great rigidity to the carbonaceous structure [99,100]. This structure is stable at 25 °C and 35 % HR (Fig. 7). When the temperature augments, the carbon fibre changes from a state of carbonisation (around 800 °C) to one of graphitization (over 900 °C) (Fig. 7), in which there are far fewer crosslinks. This allows the fibres to reorganise themselves and acquire a graphitic structure as the temperature increases [85].

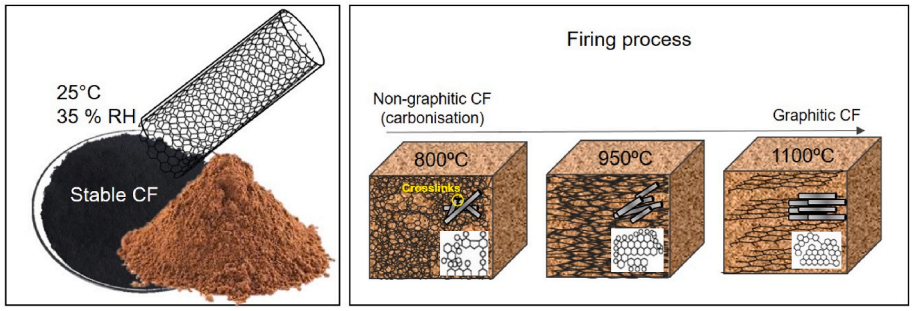

Fig. 7. Influence of temperature on the reorientation of carbon fibres.

Cameán Martinez [84] and Rodríguez Vázquez [85] demonstrated that temperatures close to 1800 °C are required for complete graphitization of the CF, although this process can be accelerated by the presence of resins and clays (as in this study), leading to further fibre orientation at 1100 °C as compared to 950 °C (Fig. 7).

3 4. *Hydric behaviour and pore system of fired bricks*

The bricks fired at 800 and 950 °C show an increase in water absorption (Ab and Af) and open porosity (Po) values with the addition of carbon fibre, changes that can also be observed in line with increases in the firing temperature (Table 4). CF0 samples showed lower values than CF5 and CF10 samples. This indicates that at low firing temperatures, the presence and amount of carbon fibre have a greater influence on the hydric behaviour of the fired pieces than the firing temperature does. The opposite trend can be observed at 1100 °C, where the addition of carbon fibre seems to hinder water absorption.

The addition of carbon fibre has a clear impact on the circulation of water in the pores and capillaries of the bricks. The bricks with no added CF achieve the best Ax values at all firing temperatures, although these values decline with the addition of CF and with increasing CF content (Table 4). Ax also worsens with the increase in the firing temperature, reaching the worst values with FC10/1100. Bricks reach high saturation indices (S, Table 4), except at 1100 °C when the extended vitrification of the ceramic mass makes them less absorbent [67]. As for drying, bricks fired at 800 °C dry faster than those fired at 950 °C, and these in turn dry faster than those fired at 1100 °C (Di, Table 4). This is logical given that pore interconnection worsens as firing temperature increases and the water finds it more difficult to move around the pore network. As regards porosity, two trends can be recognised: Po increases between 800 and 950 °C, but falls at 1100 °C (Table 4). In all cases, the presence and percentage of CF lead to higher porosity because of the imprints left by CF in the matrix of the bricks. The different behaviour at the different firing temperatures can be explained by the change in size of the carbon fibres, a process that began at 800 °C, as seen in POM and FESEM observations. This could have encouraged the development of small fissures around the fibres. Although at 1100 °C the carbon fibres underwent the same change as at 950 °C, the vitrification of the matrix was so pronounced that it hampered the development of fissures.

Water absorption by capillarity tends to increase with the addition of CF and with the rise in the firing temperature (C, Table 4). No clear trend can be observed with densities. Both, ρ_a and ρ_r are lower when CF is added, and their values fall further as higher amounts of CF are added. This is logical given the lower density of carbon fibres, as found in previous research (1.75 g cm^{-3}), compared to the silicate compounds present in the bricks.

The MIP analysis confirms the results obtained by HT (Table 4) and shows how the addition of CF modifies the pore system of the bricks in terms of open porosity and pore size distribution. All bricks display a unimodal pore size distribution with a maximum peak at around 0.1 μm (Fig. 8). The only exception is CF10/1100 which has a bimodal distribution, with a main peak between 0.1 and 1 μm and a second family of pores at around 10 μm (Fig. 8).

When comparing the different types of bricks, the maximum peak always shifts towards the right of each diagram (i.e. towards larger pores), as the firing temperature increases. This causes a reduction in the

Table 4
Hydric parameters of bricks: Ab: free water absorption (%); Af: forced water absorption (%); Ax: degree of pore interconnection (%); S: saturation coefficient (%); Di: drying index; Po: open porosity (%); C: capillarity coefficient ($g/m^2s^{0.5}$); ρ_a: apparent density (g cm^{-3}); ρ_r: real density (g cm^{-3}); MIP: Po_{MIP}: open porosity (%, determined by MIP); SSA: specific surface area (m^2 g^{-1}, determined by MIP). The standard deviation of each result is indicated in brackets.

	Hydric Test (HT)									MIP	
	Ab	Af	Ax	S	Di	Po	C	ρ_a	ρ_r	SSA	Po
CF0/800	18.30	18.96	0.21	91.73	0.92	38.46	2.09	1.84	2.93	9.65	37.23
	(4.34)	(5.37)	(1.11)	(0.89)	(0.003)	(0.66)	(1.34)	(0.02)	(0.03)	(0.07)	(1.12)
CF5/800	26.63	26.79	1.46	93.30	0.90	39.31	2.47	1.71	2.88	2.46	38.47
	(4.95)	(3.96)	(3.14)	(2.15)	(0.001)	(1.54)	(2.21)	(0.01)	(0.05)	(0.01)	(0.93)
CF10/800	32.45	32.74	19.55	92.21	0.89	40.14	2.84	1.64	2.61	2.57	41.11
	(5.84)	(0.67)	(3.22)	(1.55)	(0.012)	(3.45)	(3.44)	(0.03)	(0.05)	(0.11)	(1.25)
CF0/950	21.46	21.97	3.87	91.08	0.89	41.89	2.05	1.73	2.74	8.37	43.89
	(4.27)	(5.90)	(2.65)	(2.31)	(0.004)	(2.01)	(0.96)	(0.01)	(0.02)	(1.45)	(1.32)
CF5/950	29.87	30.09	15.79	91.74	0.90	44.96	2.38	1.56	2.48	2.21	45.11
	(5.33)	(3.89)	(5.11)	(0.94)	(0.009)	(3.65)	(3.69)	(0.03)	(0.02)	(1.88)	(2.54)
CF10/950	36.22	36.69	27.27	92.64	0.90	46.82	2.64	1.48	2.22	1.64	46.38
	(6.45)	(5.71)	(3.86)	(2.64)	(0.011)	(4.09)	(5.96)	(0.03)	(0.01)	(1.13)	(2.99)
CF0/1100	24.66	24.81	3.61	89.65	0.88	37.12	1.99	1.59	2.61	7.20	39.67
	(3.17)	(0.56)	(3.14)	(0.99)	(0.007)	(1.34)	(3.74)	(0.02)	(0.03)	(2.74)	(0.89)
CF5/1100	15.48	15.86	30.59	82.03	0.88	39.94	1.69	1.42	2.54	1.38	40.97
	(3.69)	(0.43)	(5.67)	(3.44)	(0.009)	(4.61)	(5.21)	(0.04)	(0.03)	(1.71)	(3.45)
CF10/1100	18.01	18.44	37.34	84.40	0.87	42.97	1.82	1.25	2.36	0.74	42.27
	(3.70)	(2.52)	(5.31)	(2.89)	(0.009)	(6.33)	(6.12)	(0.04)	(0.02)	(0.09)	(4.65)

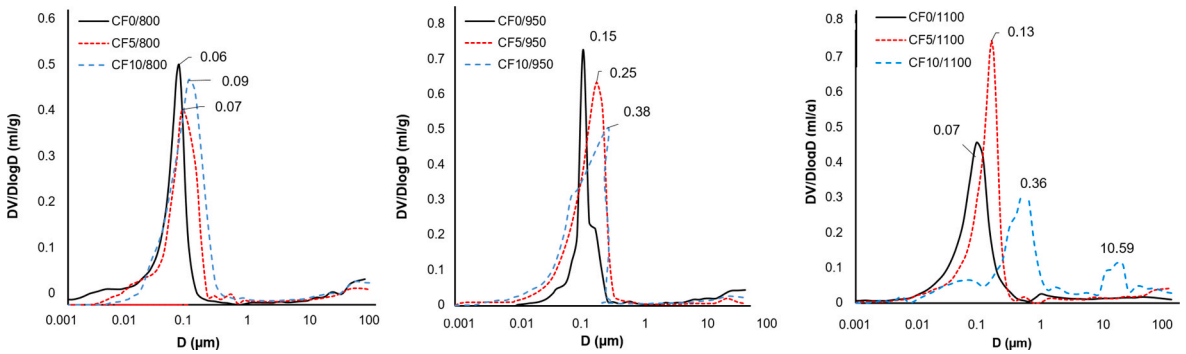

Fig. 8. MIP curves for bricks fired at 800, 950 and 1100 °C without additive (black continuous line) and with added CF (red and blue dashed lines, respectively). The pore diameter at the maximum peak in each porosimetric curve is indicated. (For interpretation of the references to colour in this figure legend, the reader is referred to the Web version of this article.)

specific surface area (SSA, Table 4) because small pores fuse into new larger ones, above all, when CF is added, leaving empty spaces in the fired bricks.

3.5. Salt crystallization test

The samples were also subjected to decay tests involving 15 salt crystallization cycles. The general trend observed in all the bricks was for an increase in weight at the beginning of the decay test, due to the presence of sodium sulphate in the pores and fissures, followed by a steep or more gradual decrease in the successive cycles. This trend was accentuated by the presence of carbon fibre. In the bricks made with added CF, after the initial crystallization of salts in the pore system (weight gain), the salts began to damage the brick, causing cracks to appear and fragments to break off (weight loss). However, at the end of the test, the samples fired at 950 and 1100 °C with added CF had suffered the least loss of material. Because of their high vitrification, the bricks fired at 1100 °C, and especially those that contain CF, lost the least weight during this experiment and are therefore considered the most durable against salt attack.

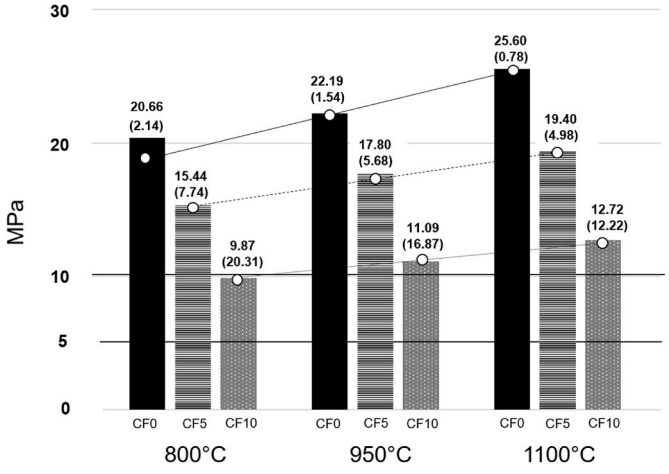

Fig. 9. Mechanical behaviour of the bricks fired at 800, 950 and 1100 °C made without additives (control group, CF0) and with added CF (CF5 and CF10). The standard deviation appears in brackets. The lines connecting the different brick types (CF0, CF5 and CF10) correspond to trend lines and the black lines at 10 and 5 MPa show minimum thresholds for solid and lightweight bricks respectively, according to the official specifications of the Spanish Ministry of Public Works [101].

3.6. Mechanical behaviour

The compressive strength of the bricks was tested according to the procedure described in Table S1 and the results of the tests are shown in Fig. 9. The addition of CF caused a progressive decline in compressive strength as compared to the control bricks, with a fall of about 25 % in samples with 5 wt% CF (CF5) and about 50 % in those with 10 wt% CF (CF10).

These results can be summarized in two main findings: i) the compressive strength of the bricks improves as the firing temperature increases; ii) the addition of carbon fibre to the clay mixture decreases the strength of the fired products. The latter is due at least in part to the increase in porosity (in CF5 and CF10) resulting from the combustion of the fibres, which causes pores to be formed (Table 4). However, the decrease in strength is much higher than the increase in porosity. This suggests that other factors may have been involved in this loss of strength. These include, firstly, the manual processing of the samples which may have resulted in CF being unevenly distributed within the clay mass (as reflected in higher standard deviation values in CF5 and CF10, Fig. 9) and secondly, the preferential orientation of the carbon fibres observed under the microscope (see Fig. 4), especially at 950 and 1100 °C, which may have reduced the compressive strength of the bricks. This shows that the results for the mechanical and thermal properties of the bricks with added CF can vary depending on the direction of measurement [102]. If we look at the three groups of samples with 0, 5 and 10 wt% of CF respectively, the mechanical strength improved as temperature increased (e.g. from 9.89 MPa to 11.07 MPa and to 12.22 MPa for samples CF10/800, CF10/950 and CF10/1100, respectively) (see Fig. 9). Thus, the highest values were found in the bricks fired at 1100 °C, with the highest compressive strength (25.6 MPa) for sample CF0/1100. This direct relationship between the firing temperature and the mechanical properties of the samples is related to their different degree of vitrification, as suggested by PXRD analysis (Table 3). These findings are consistent with earlier studies that show that compressive strength is more closely related with porosity and the degree of vitrification than with the mineralogy of the clay [103,104]. Although the addition of CF impairs the mechanical behaviour of the bricks, the results demonstrate that all the samples, with the exception of CF10/800, have sufficient compressive strength to be used for construction purposes, according to official specifications from the Spanish Ministry of Public Works [101],

3.7. Non-destructive testing of fired bricks

Table 5 shows the results of ultrasound measurements. The highest velocity values (V_p and V_s) were measured in bricks fired at 1100 °C. The presence of CF reduces the ultrasound velocity at all three firing temperatures, especially at 950 °C and 1100 °C. These results are consistent

Table 5
Average velocities (V) for the propagation of ultrasonic P and S pulses (m/s). $\bar{x}$: average values; σ: standard deviation; ΔM total anisotropy (in %); ν: Poisson's ratio; E: Young's modulus (GPa); G: shear modulus (GPa); K: bulk modulus (GPa).

	V_P (m/s)		V_S (m/s)			ν	E	G	K
	$\bar{x}$	σ	$\bar{x}$	σ	ΔM				
CF0/800	2434	2.29	1270	7.14	2.22	0.31	8.22	5.73	9.32
CF5/800	2418	51.47	1241	43.33	9.52	0.32	7.02	2.63	7.47
CF10/800	2308	278.12	1184	79.56	14.26	0.32	7.35	3.68	6.86
CF0/950	2576	3.77	1290	10.88	4.57	0.33	9.56	7.59	9.52
CF5/950	2000	76.70	1297	61.20	14.26	0.24	8.21	5.16	1.47
CF10/950	1937	212.02	1075	111.04	18.68	0.28	8.03	5.67	2.27
CF0/1100	2823	4.13	1426	12.65	7.20	0.33	10.78	6.33	7.57
CF5/1100	2693	84.27	1363	63.21	15.94	0.33	9.68	5.49	8.40
CF10/1100	2448	238.45	1871	126.34	20.46	0.20	9.99	5.61	1.90

with the lower density of the bricks fired at these two temperatures (see ρ_a and ρ_r, Table 5). The anisotropy of the bricks increased in line with increased temperature and CF content. Poisson's ratio (ν) values were very similar in all the bricks, with a small rise in the samples with added CF fired at 950 and 1100 °C. The Young modulus (E, Table 5) was higher in the control bricks (CF0) than in those with added CF. The bricks with 5 and 10 wt% CF obtained similar values at the same firing temperature. However, for all the samples, the Young modulus values increased in line with firing temperature, suggesting that firing temperature was a more important factor than the amount of CF. A similar pattern was observed in the share (G) modulus values, although the bulk modulus (K) results showed no such correlation.

The highest Leeb hardness values (LH) were observed in the bricks fired at the highest temperatures due to the high vitrification of the samples (Fig. 10). This trend was maintained with the addition of CF. Some authors [105,106] have shown that the addition of inorganic waste improves the surface hardness of fired bricks, especially at high temperatures. Fig. 10 also shows that bricks fired at 800 and 950 °C reach similar values. This confirms that the extended vitrification of the bricks occurs more between 950 and 1100 °C than between 800 and 950 °C [106]. The bricks fired at 800 °C and with added carbon fibre obtained slightly higher hardness values than those made without additive, 2.3 % higher with 5 wt% carbon fibre and 5 % with 10 wt% CF. This suggests that at 800 °C the addition of carbon fibre improves the surface hardness of the bricks very slightly. The LH results for the samples fired at 950 °C show a similar trend to those for the samples fired at 800 °C. Sometimes the values are slightly lower, possibly due to the development of small fissures described above (see Section 3.4 on hydric behaviour).

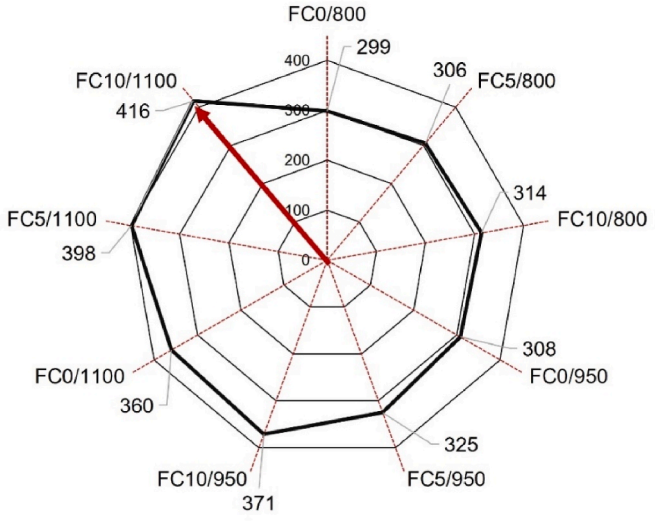

Fig. 10. Surface hardness of the bricks as determined by the Leeb Hardness Test (LH).

At 1100 °C the surface hardness of the bricks increases because of the extended vitrification as shown earlier by the POM and ultrasound techniques. The higher the carbon fibre content, the greater the increase in surface hardness. The highest hardness values were achieved by FC1100/10, with values that were 16 % higher than FC0/1100 and 32.5 % higher than FC10/800.

The fact that the surface hardness results show an opposite trend to that revealed by the compressive and ultrasonic strength tests could be due to the fact that the size and shape of both the pores and the fibres vary considerably within the brick. As we get nearer the core, the pores become larger and the fibres are shorter and thicker. This in turn confirms the heterogeneous matrix observed in the POM (Fig. 3).

3.8. Colour

According to Kreimeyer [107] and Karaman et al. [108], the colour of fired clay products is primarily determined by the type and amount of iron oxide in the clay raw material, as well as the firing temperature and the atmosphere inside the oven. Brick colour can also be affected by CaO. The presence of CaO compounds (mainly calcite) can make the bricks appear yellower because the iron is "trapped" within the structure of Ca-rich silicate phases as gehlenite, developed by the reaction between carbonates and silicates [109], and cannot develop to hematite, so causing the bricks to lose their reddish hue. Regardless of the mineralogy of the clayey material, previous authors have also shown that the use of different additives can affect the colour of the bricks [105, 110].

The bricks fired at 800 and 950 °C with or without added carbon fibre had a reddish appearance (Fig. 11). When the temperature reached 1100 °C, the difference in colour between the bricks made with and without added carbon fibre became more evident. In Fig. 10, the chromatic values (a* and b*) are divided into three different areas according to the firing temperatures. It is interesting to note that the addition of carbon fibre causes a greater dispersion of the b* parameter values. In fact, in the samples with no CF (FC0), b* ranges between 20 and 25 approximately, while in those with added CF (samples CF5 and CF10) it ranges from 5 to 30. As regards the different firing temperatures, the samples fired at 800 °C had quite homogeneous values and were grouped within a limited area, while those at 950 °C and 1100 °C were more scattered. Bricks fired at 950 °C suffer a higher variation in the a* value than in the b* value but with no marked trend in relation to the CF content. Samples fired at 1100 °C generally show lower a* and b* values and there is a marked drop in the b* value as the amount of carbon fibre augments. These bricks lose their reddish colour and turn yellow to dark-brown as the carbon fibre content increases. The lightness (L*) is not significantly affected by the firing temperature, although the lowest L* values (47.28 and 42.50, respectively) were obtained by the bricks with 5 and 10 wt% of carbon fibre fired at 1100 °C.

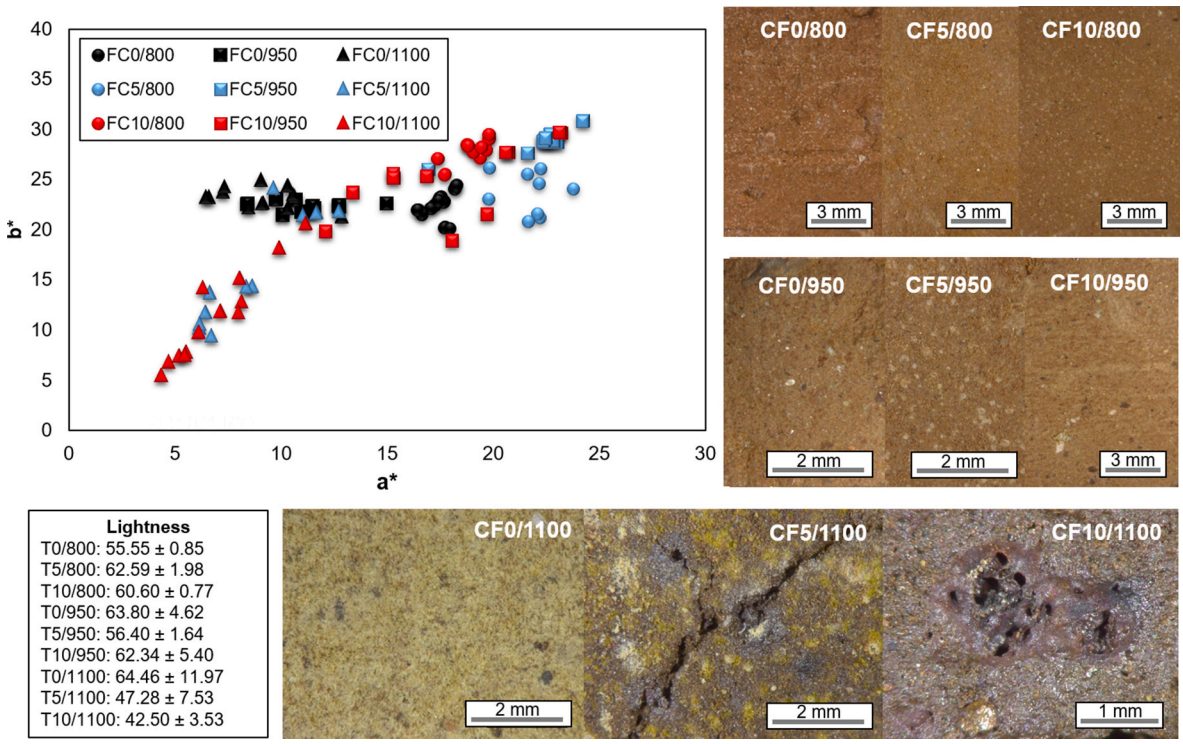

Fig. 11. Chromatic (a* and b*) and lightness (L*) values for bricks with and without added CF.The visual appearance of the nine types of bricks is shown.

3.9. Socioeconomic importance of including clay and carbon fibre in the circular economy

Red clay is a natural material used to manufacture bricks. In a recent report by the United States Geological Survey (USGS) [111], the recycling of clay was classified as "Insignificant" (U.S. Geological Survey, 2023). In those countries with an abundant supply of this material, its correct extraction and recycling can provide significant environmental and economic benefits and, in poorer countries especially, could be an important factor in their economic development.

According to the present study, the use of carbon fibres in brick-making could result in a 23 % reduction in red clay consumption (Table S1). The use of a mix composed of red clay and carbon fibre has various different benefits:

(1) Local sourcing: red clay is usually extracted from nearby quarries because it is widely available and because it is rarely viable in economic terms to source it from more distant sites, because of the high transport costs involved. Using materials in abundant supply in the immediate area not only reduces the environmental impact of transportation, but also contributes to the efficient use of regional resources.
(2) Saving natural resources: the use of 5 and 10 wt% additive would result in respective savings of 994 and 1375 kt of clay per year in Spain (a reduction in clay consumption of up to 23 %). In order to visualise what this might look like, if we assume a drilling depth of 1 m, extracting 994 and 1375 kt/year would involve quarrying an area equivalent to 110 and 152 football fields with standard dimensions of 100 m long and 50 m wide. This simple visualisation highlights the potential benefits in terms of savings in natural resources and the safeguarding of the environment.
(3) Reducing damage to the landscape: reducing the demand for clay brings environmental benefits in the area around the quarry: the impact on the landscape, the topography, and the local flora and fauna is reduced, as is the amount of dust and noise. The reduction of quarrying activity also brings several economic savings by reducing spending on explosives, electricity, labour, and the transport of materials (on conveyor belts, trucks or other vehicles).
(4) Common efforts towards sustainability: the use of carbon fibre in the brick manufacturing process would contribute to the achievement of the Sustainable Development Goals of the United Nations (SDGs, https://www.un.org/sustainabledevelopment/), and in particular SDG 9 (Industry, innovation and infrastructure) and SDG 12 (Responsible consumption and production).
(5) Physical changes: one of the main aims of materials science is to optimise certain physical properties so as to enhance the performance of the materials. Among these, the thermal conductivity of materials is important to evaluate because of its impact on their energy efficiency. The thermal conductivity of any given material is directly related to the porosity inside it. The higher the porosity, the lower the thermal conductivity because the voids act as insulating barriers, preventing heat flow. Changes in the orientation of carbon fibres and the voids left behind by them after firing can change the heat transfer inside the bricks.

However, there are also a number of drawbacks to using carbon fibre as an additive in brick production:

(1) Gas emissions: when carbon fibre is incinerated or burnt, a number of gases can be released, including carbon dioxide (CO_2) and total volatile organic compounds (TOC). CO_2 is a greenhouse gas that contributes to global warming. TOC can have adverse effects on air quality and human health, as some of these compounds can be precursors to harmful air pollutants. The presence of carbon fibre will increase CO_2 emissions into the atmosphere during firing. In addition to the negative impact on the environment, the CO_2 footprint of the finished products will be worse than that of bricks made without this residue.
(2) Quality of the final product: lower mechanical strength could make the bricks unsuitable for certain types of construction work.

It is therefore essential to verify that these materials comply with the strength requirements established in current regulations.

(3) Economic impact and difficulties in production: although some financial savings can be made by replacing part of the clayey material by a waste product, the cost of transporting the waste from the wind farms to the brick factories and the cost of grinding the residue to the size required for the brickmaking process must also be taken into account. The size of the carbon fibre particles is an important issue. The fibres used in this research were very small, which made shaping of the brick samples much easier. However, larger sizes could hinder the manufacturing process when it comes to moulding and cutting the unfired samples.

4. Conclusions

In this paper, the carbon fibre waste generated by decommissioned wind turbine blades was used as an alternative additional raw material in the production of durable bricks considered suitable for use in the construction industry and in Cultural and Architectural Heritage, so obtaining a series of important socioeconomic and environmental benefits. The most important results of this research are described below.

- It has been confirmed that carbon fibre from wind turbine blades also contains resin and thermoplastic compounds. During firing, the carbon fibre and these associated compounds are consumed, creating micropores in the bricks, so improving their thermal conductivity. On the downside, the main environmental problems arising from the manufacture of bricks with added carbon fibre are the gas emissions and unpleasant odors produced during firing. However, it is important to point out that the use of carbon fibre as an additive for brick production is less damaging, in terms of air pollution, than other "waste reduction" processes used in the wind power sector, such as incineration, pyrolysis or chemical recycling.
- The addition of carbon fibre to the clay mix partially modifies the mineralogical composition of the bricks. The concentration of hematite decreases in line with increasing firing temperature in the samples with added CF because they encourage the development of a reducing environment in the oven and the appearance of a black core.
- Texturally, the carbon fibres tend to orient themselves inside the brick. This may be influenced by the kneading and moulding of the raw bricks and by the firing temperature, as happens with the phyllosilicates.
- After firing, the carbon fibres start to degrade. As the temperature increases, they tend to disappear, leaving their imprints in the clay matrix. This increases the porosity, although the connectivity between the pores is worse in the bricks with added carbon fibre.
- Carbon fibre worsens the mechanical behaviour of the bricks. This is mainly due to their increased porosity, which was detected by analysing the porous system and the ultrasound propagation velocity. However, the samples made with CF were found to have higher surface hardness because most of the pores were in the inner part of the bricks. This could be due to the fact that the bricks were prepared by hand, which may have caused an uneven distribution of the CF particles within the clay matrix, which in turn may have affected the analysis.
- As regards the durability of the bricks, the salt crystallization test led initially to increases in weight, but with successive cycles, the bricks started to deteriorate, leading to weight loss. The presence of carbon fibre exacerbates this behaviour. However, the bricks fired at 950 and 1100 °C with added CF experienced the least material loss, making them highly resistant to salt attack and more durable.
- The colour changes resulting from CF addition did not affect the aesthetic properties of the bricks, which can make a valuable contribution as alternative building materials that are more sustainable than traditional ones.

When they reach the end of their useful life, a high percentage of turbine blades are not recycled, and have to be stored in warehouses. This could have a significant long-term impact on the environment. Within this context, the wind industry has committed to recycling or recovering 100 % of decommissioned wind blades by 2025. In addition, wind turbines are becoming larger in order to be able to generate more power per turbine. This requires larger installations, with some prototypes reaching up to 280 m in height. These huge turbines have 116-m-long blades, which can produce up to 16 MW (MW), enough to power 20,000 homes over their 25-year lifespan. In recent decades, the capacity of wind power installations worldwide has grown steadily from 24 GW (GW) in 2001 to 837 GW in 2022, with China, the United States of America, Germany, India and Spain accounting for 72 % of global wind power installations. In terms of the number of wind turbines, Spain has 21,574 wind turbines (Asociación Empresarial Eólica), while the United States has 72,731.

The use of carbon fibre in the manufacture of bricks could therefore provide an excellent opportunity for both the reduction of clay consumption and the reuse of carbon fibre from wind turbine blades, so designing a circular economy process with two main benefits. Firstly, the use of raw materials (in this case clay) is minimized and secondly, the waste (carbon fibre) generated in a process, wind energy production, that is essential in the fight against climate change can be reused as an alternative building material. The results show that reusing carbon fibre waste from wind turbine blades in brick manufacture has great potential as part of a strategy for achieving the goals of the 2030 Agenda for Sustainable Development.

Funding for open access charge

Universidad de Granada/CBUA.

Declaration of competing interest

The authors declare that they have no known competing financial interests or personal relationships that could have appeared to influence the work reported in this paper.

Acknowledgements

This study has been funded by Junta de Andalucía Research Group RNM179 and by Research Project B-RNM-188-UGR20 of the Regional Ministry of University, Research and Innovation of the Junta de Andalucía and FEDER, *a way of making Europe*. We are grateful to Nigel Walkington for his assistance in revising the English text of the manuscript. We also thank Tesela, Materiales, Innovación y Patrimonio S.L. (https://teselainnova.com/), who supplied the carbon fibre powder, and Cerámica Castillo Siles (www.ceramicacastillosiles.es), who provided the raw material.

Thanks also to the Department of Geosciences of the University of Padova and in particular to Dr. Chiara Dalconi for her assistance during the Rietveld methodology and Giampaolo Girardi for his assistance during the compression test.

Appendix A. Supplementary data

Supplementary data to this article can be found online at https://doi.org/10.1016/j.ceramint.2023.12.287.

References

[1] W.R. Stahel, The circular economy, Nature 531 (7595) (2016) 435–438, https://doi.org/10.1038/531435a.

[2] S. Geisendorf, F. Pietrulla, The circular economy and circular economic concepts a literature analysis and redefinition, Thunderbird Int. Bus. Rev. 60 (5) (2018) 771–782, https://doi.org/10.1002/tie.21924.

[3] K. Webster, A circular economy is about the economy, Circ. Econ. Sust. 1 (1) (2021) 115–126, https://doi.org/10.1007/s43615-021-00034-z.
[4] H. Corvellec, A.F. Stowell, N. Johansson, Critiques of the circular economy, J. Ind. Ecol. 26 (2) (2022) 421–432, https://doi.org/10.1111/jiec.13187.
[5] UN General Assembly, Transforming Our World: the 2030 Agenda for Sustainable Development. A/RES/70/1, 2015. Available at: https://www.refworld.org/docid/57b6e3e44.html. July 2023.
[6] GWEC, Global Wind Report 2022, 2022. https://gwec.net/wp-content/uploads/2022/03/GWEC-GLOBAL-WIND-REPORT-2022.pdf. July 2023.
[7] O. Gencel, M.J. Munir, S.M.S. Kazmi, M. Sutcu, E. Erdogmus, P.M. Velasco, D. E. Quesada, Recycling industrial slags in production of fired clay bricks for sustainable manufacturing, Ceram. Int. 47 (21) (2021) 30425–30438, https://doi.org/10.1016/j.ceramint.2021.07.222.
[8] O. Gencel, S.M.S. Kazmi, M.J. Munir, M. Sutcu, E. Erdogmus, A. Yaras, Feasibility of using clay-free bricks manufactured from water treatment sludge, glass, and marble wastes: an exploratory study, Construct. Build. Mater. 298 (2021), 123843, https://doi.org/10.1016/j.conbuildmat.2021.123843.
[9] Y. Er, M. Sutcu, O. Gencel, E. Totic, E. Erdogmus, V.V. Cay, S.M.S. Kazmi, Recycling of metallurgical wastes in ceramics: a sustainable approach, Construct. Build. Mater. 349 (2022), 128713, https://doi.org/10.1016/j.conbuildmat.2022.128713.
[10] L. Crespo-López, G. Cultrone, Improvement in the petrophysical properties of solid bricks by adding household glass waste, J. Build. Eng. 59 (2022), 105039, https://doi.org/10.1016/j.jobe.2022.105039.
[11] E. Erdogmus, M. Sutcu, O. Gencel, S.M.S. Kazmi, M.J. Munir, P.M. Velasco, T. Ozbakkaloglu, Enhancing thermal efficiency and durability of sintered clay bricks through incorporation of polymeric waste materials, J. Clean. Prod. 420 (2023), 138456, https://doi.org/10.1016/j.jclepro.2023.138456.
[12] REPowerEU. Available at: https://commission.europa.eu/[accessed July 2023].
[13] M. Arshad, B. O'Kelly, Global status of wind power generation: theory, practice, and challenges, Int. J. Green Energy 16 (14) (2019) 1073–1090, https://doi.org/10.1080/15435075.2019.1597369.
[14] G.W.E. Council, Global offshore wind report 2020, GWEC: Brussels, Belgium 19 (2020) 10–12.
[15] A.R. Kalair, M. Seyedmahmoudian, A. Stojcevski, N. Abas, N. Khan, Waste to energy conversion for a sustainable future, Heliyon 7 (10) (2021), https://doi.org/10.1016/j.heliyon.2021.e08155.
[16] T. Higuchi, M. Morioka, I. Yoshioka, K. Yokozeki, Development of a new ecological concrete with CO2 emissions below zero, Construct. Build. Mater. 67 (2014) 338–343, https://doi.org/10.1016/j.conbuildmat.2014.01.029.
[17] J.S. González, R. Lacal-Arántegui, A review of regulatory framework for wind energy in European Union countries: current state and expected developments, Renew. Sustain. Energy Rev. 56 (2016) 588–602, https://doi.org/10.1016/j.rser.2015.11.091.
[18] P. Bórawski, A. Bełdycka-Bórawska, K.J. Jankowski, B. Dubis, J.W. Dunn, Development of wind energy market in the European Union, Renew. Energy 161 (2020) 691–700, https://doi.org/10.1016/j.renene.2020.07.081.
[19] M. Ruska, J. Kiviluoma, Renewable Electricity in Europe. Current State, Drivers, and Scenarios for 2020, 2011.
[20] The International Energy Agency, IEA, 2020. Available at: https://www.iea.org/reports/world-energy-outlook-2020. July 2023.
[21] WindEurope, Available at: https://windeurope.org/, 2021. July 2023.
[22] European wind energy association (EWEA), Available at: https://www.ewea.org/. September 2023].
[23] Recycling international, Available at: https://recyclinginternational.com/. September 2023.
[24] M. Rani, P. Choudhary, V. Krishnan, S. Zafar, A review on recycling and reuse methods for carbon fiber/glass fiber composites waste from wind turbine blades, Compos. B Eng. 215 (2021), 108768, https://doi.org/10.1016/j.compositesb.2021.108768.
[25] D. Song, Z. Li, L. Wang, F. Jin, C. Huang, E. Xia, R.M. Rizk-Allah, J. Yang, M. Su, Y.H. Joo, Energy capture efficiency enhancement of wind turbines via stochastic model predictive yaw control based on intelligent scenarios generation, Appl. Energy 312 (2022), 118773, https://doi.org/10.1016/j.apenergy.2022.118773.
[26] L. Mishnaevsky Jr., K. Branner, H.N. Petersen, J. Beauson, M. McGugan, B. F. Sørensen, Materials for wind turbine blades: an overview, Materials 10 (11) (2017) 1285, https://doi.org/10.3390/ma10111285.
[27] L. Thomas, M. Ramachandra, Advanced materials for wind turbine blade-A Review, Mater. Today: Proc. 5 (1) (2018) 2635–2640, https://doi.org/10.1016/j.matpr.2018.01.043.
[28] K. Kalkanis, C.S. Psomopoulos, S. Kaminaris, G. Ioannidis, P. Pachos, Wind turbine blade composite materials-End of life treatment methods, Energy Proc. 157 (2019) 1136–1143, https://doi.org/10.1016/j.egypro.2018.11.281.
[29] S. Hao, A.T. Kuah, C.D. Rudd, K.H. Wong, N.Y.G. Lai, J. Mao, X. Liu, A circular economy approach to green energy: wind turbine, waste, and material recovery, Sci. Total Environ. 702 (2020), 135054, https://doi.org/10.1016/j.scitotenv.2019.135054.
[30] H. Albers, S. Greiner, H. Seifert, U. Kühne, Recycling of wind turbine rotor blades. Fact or fiction?, in: Recycling von Rotorblaettern aus Windenergieanlagen. Fakt oder Fiktion? DEWI-Magazin, 2009.
[31] M.R. Sanjay, P. Madhu, M. Jawaid, P. Senthamaraikannan, S. Senthil, S. Pradeep, Characterization and properties of natural fiber polymer composites: a comprehensive review, J. Clean. Prod. 172 (2018) 566–581, https://doi.org/10.1016/j.jclepro.2017.10.101.
[32] A. Yazdanbakhsh, L.C. Bank, K.A. Rieder, Y. Tian, C. Chen, Concrete with discrete slender elements from mechanically recycled wind turbine blades, Resour. Conserv. Recycl. 128 (2018) 11–21, https://doi.org/10.1016/j.resconrec.2017.08.005.
[33] M. Dabaieh, Brick production: environmental impacts and alternatives, J. Clean. Prod. 243 (2020), 118590.
[34] M. Dabaieh, J. Heinonen, D. El-Mahdy, D.M. Hassan, A comparative study of life cycle carbon emissions and embodied energy between sun-dried bricks and fired clay bricks, J. Clean. Prod. 275 (2020), 122998, https://doi.org/10.1016/j.jclepro.2020.122998.
[35] S.A. Babatunde, Review of strengthening techniques for masonry using fiber reinforced polymers, Compos. Struct. 161 (2017) 246–255, https://doi.org/10.1016/j.compstruct.2016.10.132.
[36] C. Vega, N. Torres, External strengthening of unreinforced masonry walls with polymers reinforced with carbon fiber, Ing. Invest. 38 (3) (2018) 15–23, https://doi.org/10.15446/ing.investig.v38n3.73151.
[37] B. Kromoser, P. Preinstorfer, J. Kollegger, Building lightweight structures with carbon-fiber-reinforced polymer-reinforced ultra-high-performance concrete: research approach, construction materials, and conceptual design of three building components, Struct. Concr. 20 (2) (2019) 730–744, https://doi.org/10.1002/suco.201700225.
[38] A. García-Alix, R. Minwer-Barakat, J.M. Martín, E. Martín-Suárez, M. Freudenthal, Biostratigraphy and sedimentary evolution of late Miocene and Pliocene continental deposits of the Granada Basin (southern Spain), Lethaia 41 (2008) 431–446, https://doi.org/10.1111/j.1502-3931.2008.00097.x.
[39] R.T. Laird, M. Worcester, The inhibiting of lime blowing, Transactions of the Br. Ceram. Trans. 55 (1956) 545–563.
[40] S.I. Tsipursky, V.A. Drits, The distribution of octahedral cations in the 2:1 layers of dioctahedral smectites studied by oblique-texture electron diffraction, Clay Miner. 19 (1984) 177–193, https://doi.org/10.1180/claymin.1984.019.2.05.
[41] T. Taut, R. Kleeberg, J. Bergmann, The new seifert rietveld program BGMN and its application to quantitative phase analysis, Mater. Struct. 5 (1) (1998) 55–64.
[42] K. Ufer, G. Roth, R. Kleeberg, H. Stanjek, R. Dohrmann, J. Bergmann, Description of X-ray powder pattern of turbostratically disordered layer structures with a Rietveld compatible approach, Z. Kristallogr. 219 (2004) 519–527, https://doi.org/10.1524/zkri.219.9.519.44039.
[43] N. Kleeberg Dobelin, R. Profex, A graphical user interface for the Rietveld refinement program BGMN, J. Appl. Crystallogr. 48 (2015) 1573–1580, https://doi.org/10.1107/S1600576715014685.
[44] H.M. Rietveld, A profile refinement method for nuclear and magnetic structures, J. Appl. Crystallogr. 2 (1969) 65–71, https://doi.org/10.1107/S0021889869006558.
[45] UNE-EN 13755, Métodos de ensayo para piedra natural. Determinación de la absorción de agua a presión atmosférica, AENOR, Madrid, 2008.
[46] NORMAL 19/88, Misura dell'indice di asciugamento (drying index), CNR-ICR, Roma, Italia, 1988.
[47] UNE-EN 1926, Métodos de ensayo para piedra natural. Determinación del coeficiente de absorción de agua por capilaridad, AENOR, Madrid, 2007.
[48] RILEM, Recommended tests to measure the deterioration of stone and to assess the effectiveness of treatment methods. Commision 25-PEM: protection et Erosion des Monuments, Mater. Struct. 13 (75) (1980) 175–253.
[49] UNE-EN 1936, Métodos de ensayo para piedra natural. Determinación de la densidad real y aparente y de la porosidad abierta y total, AENOR, Madrid, 2007.
[50] ISRM, Suggested methods for determining water content, porosity, density and related properties, and swelling, Int. J. Rock Mech. Min. Sci. 16 (2) (1979) 141–156.
[51] UNE-EN 12370, Métodos de ensayo para piedra natural. Determinación de la resistencia a la cristalización de sales, AENOR, Madrid, 2002.
[52] UNE-EN 196-1, Métodos de ensayo de cementos. Parte 1: Determinación de resistencias mecánicas, AENOR, Madrid, 2005.
[53] ASTM D2845, Standard Test Method for Laboratory Determination of Pulse Velocities and Ultrasonic Elastic Constants of Rock, J. ASTM Int., West Conshohocken, PA, USA, 2000.
[54] G. Cultrone, E. Sebastián, Fly ash addition in clayey materials to improve the quality of solid bricks, Construct. Build. Mater. 23 (2) (2009) 1178–1184, https://doi.org/10.1016/j.conbuildmat.2008.07.001.
[55] C. Coletti, G. Cultrone, L. Maritan, C. Mazzoli, How to face the new industrial challenge of compatible, sustainable brick production: study of various types of commercially available bricks, Appl. Clay Sci. 124 (2016) 219–226, https://doi.org/10.1016/j.clay.2016.02.01.
[56] G.N. Pande, J.X. Liang, J. Middleton, Equivalent elastic moduli for brick masonry, Comput. Geotech. 8 (3) (1989) 243–265, https://doi.org/10.1016/0266-352X(89)90045-1.
[57] L. Crespo-López, D. Benavente, S. Morales-Ruano, M. Vázquez-Vílchez, G. Cultrone, Non-destructive techniques (NDT) and statistical analysis for the characterization of bricks made with added glass, Construct. Build. Mater. 408 (2023), 133583, https://doi.org/10.1016/j.conbuildmat.2023.133583.
[58] UNE-EN 15886, Métodos de ensayo. Medición del color de superficies, AENOR, Madrid, 2011.
[59] L. Maritan, L. Nodari, C. Mazzoli, A. Milano, U. Russo, Influence of firing conditions on ceramic products: experimental study on clay rich in organic matter, Appl. Clay Sci. 31 (1–2) (2006) 1–15, https://doi.org/10.1016/j.clay.2005.08.007.
[60] M. Labus, Thermal methods implementation in analysis of fine-grained rocks containing organic matter, J. Therm. Anal. Calorim. 129 (2) (2017) 965–973, https://doi.org/10.1007/s10973-017-6259-7.
[61] J.M. Fernández, C. Peltre, J.M. Craine, A.F. Plante, Improved characterization of soil organic matter by thermal analysis using CO_2/H_2O evolved gas analysis,

Environ. Sci. Amp. Technol. 46 (16) (2012) 8921–8927, https://doi.org/10.1021/es301375d.
[62] M. Coquelle, Flame Retardancy of Polyamide 6 Fibers: the Use of Sulfamate Salts, 2014. Doctoral dissertation, Lille 1).
[63] G. Cultrone, C. Rodriguez-Navarro, E. Sebastian, O. Cazalla, M.J. De La Torre, Carbonate and silicate phase reactions during ceramic firing, Eur. J. Mineral 13 (3) (2001) 621–634, https://doi.org/10.1127/0935-1221/2001/0013-0621.
[64] C. Rodriguez-Navarro, E. Ruiz-Agudo, A. Luque, A.B. Rodriguez-Navarro, M. Ortega-Huertas, Thermal decomposition of calcite: mechanisms of formation and textural evolution of CaO nanocrystals, Am. Mineral. 94 (4) (2009) 578–593, https://doi.org/10.2138/am.2009.3021.
[65] C. Rodriguez-Navarro, K. Kudlacz, E. Ruiz-Agudo, The mechanism of thermal decomposition of dolomite: new insights from 2D-XRD and TEM analyses, Am. Mineral. 97 (1) (2012) 38–51, https://doi.org/10.2138/am.2011.3813.
[66] L. Heller-Kallai, I. Lapides, Dehydroxylation of muscovite: study of quenched samples, Phys. Chem. Miner. 42 (10) (2015) 835–845, https://doi.org/10.1007/s00269-015-0767-4.
[67] G. Cultrone, E. Sebastián, K. Elert, M.J. De la Torre, O. Cazalla, C. Rodriguez–Navarro, Influence of mineralogy and firing temperature on the porosity of bricks, J. Eur. Ceram. Soc. 24 (3) (2004) 547–564, https://doi.org/10.1016/S0955-2219(03)00249-8.
[68] T. Hirono, W. Tanikawa, Implications of the thermal properties and kinetic parameters of dehydroxylation of mica minerals for fault weakening, frictional heating, and earthquake energetics, Earth Planet Sci. Lett. 307 (1–2) (2011) 161–172, https://doi.org/10.1016/j.epsl.2011.04.042.
[69] A.C. Boccara, D. Fournier, A. Kumar, G.C. Pandey, Nondestructive evaluation of carbon fiber by mirage-FTIR spectroscopy, J. Appl. Polym. Sci. 63 (13) (1997) 1785–1791, https://doi.org/10.1002/(SICI)1097-4628(19970328)63:13<1785::AID-APP11>3.0.CO;2-Y.
[70] S. Shin, J. Jang, S.H. Yoon, I. Mochida, A study on the effect of heat treatment on functional groups of pitch based activated carbon fiber using FTIR, Carbon 35 (12) (1997) 1739–1743, https://doi.org/10.1016/S0008-6223(97)00132-2.
[71] S.B. Hanna, A.A. Yehia, M.N. Ismail, A.I. Khalaf, Preparation and characterization of carbon fibers from polyacrylonitrile precursors, J. Appl. Polym. Sci. 123 (4) (2012) 2074–2083, https://doi.org/10.1002/app.34704.
[72] C. Sellitti, J.L. Koenig, H. Ishida, Surface characterization of graphitized carbon fibers by attenuated total reflection Fourier transform infrared spectroscopy, Carbon 28 (1) (1990) 221–228, https://doi.org/10.1016/0008-6223(90)90116-G.
[73] M. Starsinic, R.L. Taylor, P.L. Walker Jr., P.C. Painter, FTIR studies of Saran chars, Carbon 21 (1) (1983) 69–74, https://doi.org/10.1016/0008-6223(83)90158-6.
[74] A.B.D. Nandiyanto, R. Oktiani, R. Ragadhita, How to read and interpret FTIR spectroscope of organic material, Indonesian J. Sci. Technol. 4 (1) (2019) 97–118, https://doi.org/10.17509/ijost.v4i1.15806.
[75] A.P.C. Barbosa, A.P.P. Fulco, E.S. Guerra, F.K. Arakaki, M. Tosatto, M.C.B. Costa, J.D.D. Melo, Accelerated aging effects on carbon fiber/epoxy composites, Compos. B Eng. 110 (2017) 298–306, https://doi.org/10.1016/j.compositesb.2016.11.004.
[76] L. Guan, H. Xu, D. Huang, The investigation on states of water in different hydrophilic polymers by DSC and FTIR, J. Polym. Res. 18 (2011) 681–689, https://doi.org/10.1007/s10965-010-9464-7.
[77] S. Süzer, L. Andrews, FTIR spectra of ammonia clusters in noble gas matrices, The J. chem.phys. 87 (9) (1987) 5131–5140, https://doi.org/10.1063/1.453681.
[78] L.V. Cremades, C. Soriano, J.A. Cusidó, Tackling environmental issues in industrial ceramic sintering of sewage sludge: odors and gas emissions, Environ. Dev. Sustain. 20 (2018) 1651–1663, https://doi.org/10.1007/s10668-017-9958-0.
[79] I. Poljansek, M. Krajnc, Characterization of phenol-formaldehyde prepolymer resins by in line FT-IR spectroscopy, Acta Chim. Slov. 52 (3) (2005) 238.
[80] J.A. Cusidó, L.V. Cremades, M. González, Gaseous emissions from ceramics manufactured with urban sewage sludge during firing processes, Waste Manage. (Tucson, Ariz.) 23 (3) (2003) 273–280, https://doi.org/10.1016/S0956-053X(02)00060-0.
[81] S. Karavida, R. Nõmmik, Waste Management of End-Of-Service Wind Turbines. (PhD Dissertation), Aalborg University, 2015.
[82] P. Majewski, N. Florin, J. Jit, R.A. Stewart, End-of-life policy considerations for wind turbine blades, Renew. Sustain. Energy Rev. 164 (2022), 112538, https://doi.org/10.1016/j.rser.2022.112538.
[83] D. Martinez-Marquez, N. Florin, W. Hall, P. Majewski, H. Wang, R.A. Stewart, State-of-the-art review of product stewardship strategies for large composite wind turbine blades, Resour., Conserv. Recycl. Adv. (2022), 200109, https://doi.org/10.1016/j.rcradv.2022.200109.
[84] I. Cameán, Preparación de materiales grafíticos: aplicación como ánodos en baterías de ión-litio (Doctoral dissertation, Universidad de Oviedo, 2011.
[85] E. Rodríguez Vázquez, Espumas de carbono con propiedades avanzadas derivadas de carbones bituminosos. (Doctoral dissertation, Universidad de Oviedo, 2014.
[86] M.D.R. Cruz, Na-bearing white micas from Triassic rocks of the transition between the Malaguide and Alpujarride complexes (Betic Cordillera, Spain), Clay Clay Miner. 56 (3) (2008) 344–358, https://doi.org/10.1346/CCMN.2008.0560305.
[87] J. Jiménez-Millán, I. Abad, F.J. García-Tortosa, R. Jiménez-Espinosa, Structural diagenesis in clay smearing bands developed on plio-pleistocene sediments affected by the baza fault (S Spain), Minerals 12 (10) (2022) 1255, https://doi.org/10.3390/min12101255.
[88] J. Martin, M. Ortega-Huertas, J. Torres-Ruiz, Genesis and evolution of strontium deposits of the Granada Basin (southeastern Spain): evidence of diagenetic replacement of a stromatolite belt, Sediment. Geol. 39 (3–4) (1984) 281–298, https://doi.org/10.1016/0037-0738(84)90055-1.
[89] L.N. Warr, Recommended abbreviations for the names of clay minerals and associated phases, Clay Miner. 55 (3) (2020) 261–264, https://doi.org/10.1180/clm.2020.30.
[90] W.D. Kingery, H.K. Bowen, D.R. Uhlmann, Introduction to Ceramics, vol. 17, John wiley & sons, 1976.
[91] J.R. Goldsmith, F. Laves, The microcline-sanidine stability relations, Geochem. Cosmochim. Acta 5 (1) (1954) 1–19, https://doi.org/10.1016/0016-7037(54)90058-7.
[92] J.A. Pask, A.P. Tomsia, Formation of mullite from sol-gel mixtures and kaolinite, J. Am. Ceram. Soc. 74 (10) (1991) 2367–2373, https://doi.org/10.1111/j.1151-2916.1991.tb06770.x.
[93] C. Rodriguez-Navarro, G. Cultrone, A. Sanchez-Navas, E. Sebastian, TEM study of mullite growth after muscovite breakdown, Am. Mineral. 88 (5–6) (2003) 713–724, https://doi.org/10.2138/am-2003-5-601.
[94] J.J. Vilatela, M.E. Rabanal, F. Cervantes-Sodi, M. García-Ruiz, J.A. Jiménez-Rodríguez, G. Reiband, M. Terrones, A spray pyrolysis method to grow carbon nanotubes on carbon fibres, steel and ceramic bricks, J. Nanosci. Nanotechnol. 15 (4) (2015) 2858–2864, https://doi.org/10.1166/jnn.2015.9601.
[95] S. Sharma, K.K. Wetzel, Process development issues of glass-carbon hybrid-reinforced polymer composite wind turbine blades, J. Compos. Mater. 44 (4) (2010) 437–456, https://doi.org/10.1177/0021998309347569.
[96] K. Debnath, I. Singh, A. Dvivedi, P. Kumar, Natural fibre-reinforced polymer composites for wind turbine blades: challenges and opportunities, in: Recent Advances in Composite Materials for Wind Turbine Blades, 2013.
[97] E. Linul, L. Marsavina, Mechanical characterization of rigid pur foams used for wind turbine blades construction, in: Recent Advances in Composite Materials for Wind Turbines Blades, WAP-AMSA, 2013.
[98] G. Cultrone, F.J.C. Rosua, Growth of metastable phases during brick firing: mineralogical and microtextural changes induced by the composition of the raw material and the presence of additives, Appl. Clay Sci. 185 (2020), 105419, https://doi.org/10.1016/j.clay.2019.105419.
[99] P.L. Walker Jr., R.L. Taylor, J.M. Ranish, An update on the carbon-oxygen reaction, Carbon 29 (3) (1991) 411–421, https://doi.org/10.1016/0008-6223(91)90210-A.
[100] L.R. Radovic, Carbons and graphites, reactivity of, Encyclopedia of materials: Sci. Technol. (2001) 975–984, https://doi.org/10.1016/B0-08-043152-6/00182-0.
[101] R.L.-88 Pliego, Pliego General de Condiciones para la Recepción de Ladrillos Cerámicos en las Obras de Construcción, Ministerio de Obras Públicas, Transportes y Medio Ambiente, Spain, 1988.
[102] H.O. Pierson, Graphite structure and properties. Handbook of carbon, graphite, diamonds and fullerenes (1993) 43–69.
[103] P. Saravanapavan, L.L. Hench, Mesoporous calcium silicate glasses. I. Synthesis, J. Non-Cryst. Solids 318 (1–2) (2003) 1–13, https://doi.org/10.1016/S0022-3093(02)01864-1.
[104] M. Dondi, G. Guarini, M. Raimondo, C. Zanelli, Recycling PC and TV waste glass in clay bricks and roof tiles, J. Waste Manag. 29 (6) (2009) 1945–1951, https://doi.org/10.1016/j.wasman.2008.12.003.
[105] L. Crespo-López, A. Martínez-Ramirez, E. Sebastián, G. Cultrone, Pomace from the wine industry as an additive in the production of traditional sustainable lightweight eco-bricks, Appl. Clay Sci. 243 (2023), 107084, https://doi.org/10.1016/j.clay.2023.107084.
[106] C. Coletti, L. Maritan, G. Cultrone, M.C. Dalconi, A. Hein, E. Molina, C. Mazzoli, Recycling trachyte waste from the quarry to the brick industry: effects on physical and mechanical properties, and durability of new bricks, Construct. Build. Mater. 166 (2018) 792–807, https://doi.org/10.1016/j.conbuildmat.2018.01.158.
[107] R. Kreimeyer, Some notes on the firing colour of clay bricks, Appl. Clay Sci. 2 (2) (1987) 175–183, https://doi.org/10.1016/0169-1317(87)90007-X.
[108] S. Karaman, H. Gunal, S. Ersahin, Assesment of clay bricks compressive strength using quantitative values of colour components, Construct. Build. Mater. 20 (5) (2006) 348–354, https://doi.org/10.1016/j.conbuildmat.2004.11.003.
[109] Y. Maniatis, A. Simopoulos, A. Kostikas, V. Perdikatsis, Effect of reducing atmosphere on minerals and iron oxides developed in fired clays: the role of Ca, J. Am. Ceram. Soc. 66 (11) (1983) 773–781, https://doi.org/10.1111/j.1151-2916.1983.tb10561.x.
[110] N. Saenz, E. Sebastián, G. Cultrone, Analysis of tempered bricks: from raw material and additives to fired bricks for use in construction and heritage conservation, Eur. J. Mineral 31 (2) (2019) 301–312, https://doi.org/10.1127/ejm/2019/0031-2832.
[111] U.S. Geological Survey, Mineral Commodity Summaries 2023, U.S. Geological Survey, 2023, p. 210, https://doi.org/10.3133/mcs2023 [09/07/2023].